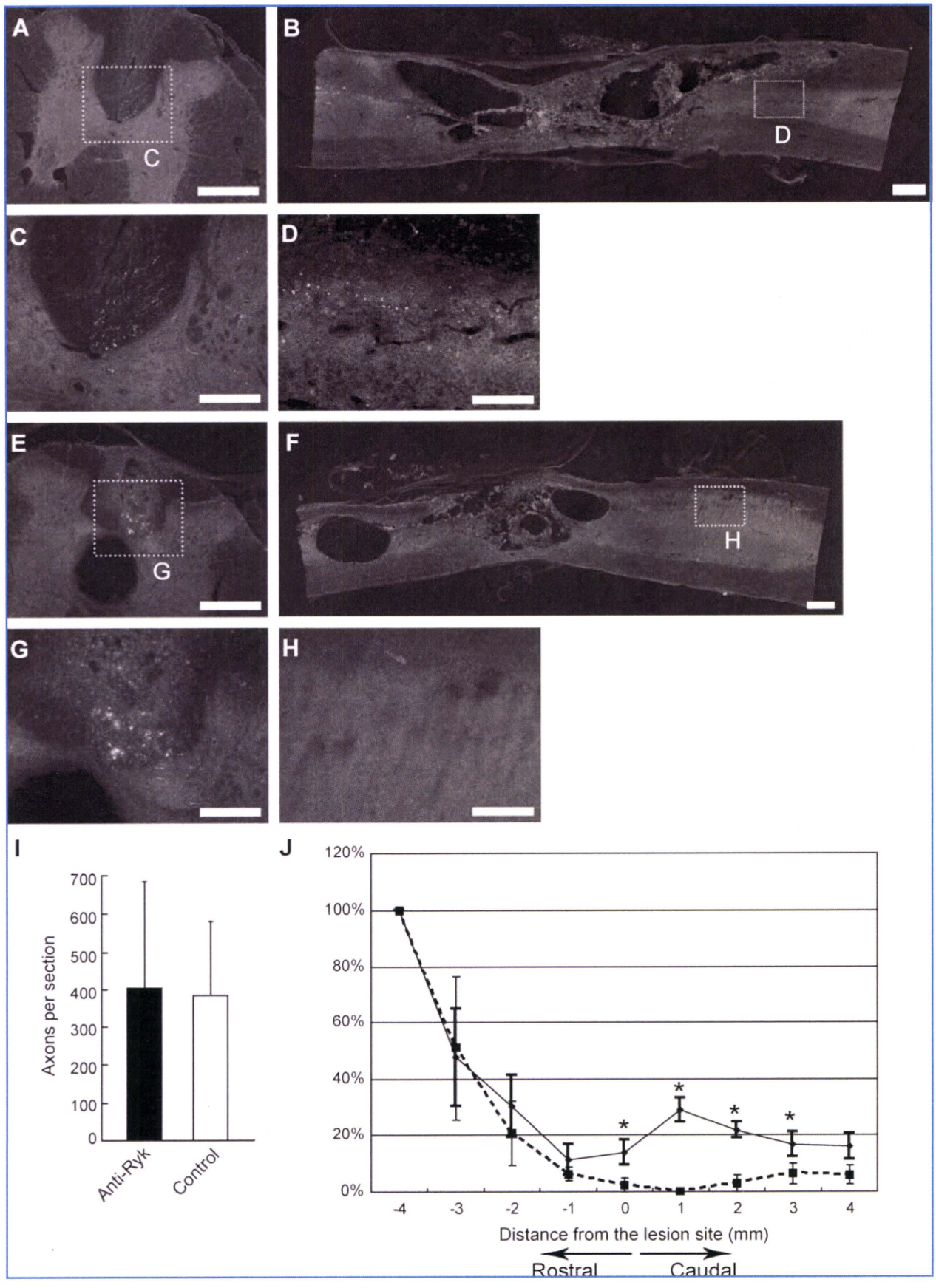
A
B
C
D
C
D
E
F
G
H
G
H
I
Axons per section
700
600
500
400
300
200
100
0
Anti-Ryk
Control
J
120%
100%
80%
60%
40%
20%
0%
-4
-3
-2
-1
0
1
2
3
4
Distance from the lesion site (mm)
Rostral
Caudal

required for the inhibitory effect of Wnt-5a on CGN neurite growth.

Ryk neutralization leads to functional improvement

The binding of Wnts to Ryk repels CST axons during the developmental stages both *in vitro* and *in vivo* (Liu et al., 2005), and Ryk is expressed in the CST of adult rats after SCI (Fig. 1X,Y). The above-mentioned results suggest the possibility that Wnt proteins, by virtue of their ability to inhibit neurite outgrowth, act as a barrier to the regrowth of injured axons after SCI, and that the blockage of these proteins may enhance recovery after SCI. We employed a rat spinal contusion model since this is relevant to clinical conditions. The spinal cords at the thoracic level (Th9/10) were contused by an impactor. The anti-Ryk antibody or a rabbit IgG control was administered for 2 weeks via osmotic minipumps connected to intrathecal catheters placed near the thoracic injury site. The locomotor performance of the animals was monitored over an 8-week period after the injury. The sham-operated rats (Fig. 3) achieved full scores according to the BBB locomotor rating scale (Basso et al., 1995). All rats with a SCI became almost completely paraplegic from days 1–3 after the injury. As indicated by their BBB scores, these animals gradually exhibited partial recovery of locomotor behavior (Fig. 3). At 2–8 weeks after the injury, the locomotor performance of rats treated with the anti-Ryk antibody tended to exhibits a better recovery than in those treated with the control IgG. On average, the control IgG-treated rats attained a BBB score of 12.0, whereas those treated with the anti-Ryk antibody achieved a significantly higher BBB score of 14.2 at 8 weeks after the surgery (Fig. 3). Thus, the anti-Ryk antibody treatment significantly improved locomotor recovery following the spinal cord contusion in rats.

Ryk inhibition induces growth of injured corticospinal fiber tracts

Finally, we examined whether Wnt-Ryk signaling contributes to the inhibition of axon regeneration/sprouting after the SCI. The integrity of the dorsal CST in previously tested rats was assessed by injecting BDA into the unilateral sensorymotor cortex. The total number of labeled fibers located 10 mm above the lesion was not different between the anti-Ryk antibody-treated and the control IgG-treated rats (Fig. 4A,C,E,G,I), thus indicating that the extent of BDA uptake was identical between the groups. For a group of animals (four control and seven anti-Ryk antibody-treated rats), blocks that extended 5 mm rostral and 5 mm caudal to the center of the injury were sectioned in the sagittal plane (Fig. 4B,F). It is notable that labeled fibers with typical irregular meandering growth patterns were frequently observed in the tissue caudal to the lesion in the anti-Ryk antibody-treated rats (Fig. 4B,D), whereas no BDA-labeled CST fibers were detected in the control IgG-treated rats (Fig. 4F,H). We then reconstructed the transverse sections of the injured spinal cord and estimated the number of labeled fibers. Compared to the number of labeled fibers that were observed 4 mm rostral to the lesion site, more than 20% of the labeled fibers were observed 1–2 mm caudal to the lesion epicenter in the anti-Ryk antibody-treated rats. However, only a small percentage of the labeled fibers (0% at 1 mm and 3% at 2 mm caudal to the injury site) were observed in the control IgG-treated rats (Fig. 4J). Labeled fibers were detected in the gray matter of injured animals treated with the anti-Ryk antibody (Fig. 4D). Since we observed no labeled fibers in the normal locations of the dorsal CST caudal to the lesion site in any of the injured rats (data not shown), the increase in the labeled fibers after the anti-Ryk antibody treatment was not due to an increased survival of the dorsal CST. Thus, these results demonstrate that treatment with the anti-Ryk antibody promoted significant fiber growth from the intact ventral CST or the injured dorsal CST after SCI. Ryk appears to mediate the inhibition of CST axon growth following SCI.

Discussion

Our study demonstrates that Wnt-5a was induced in the reactive astrocytes surrounding the site of injury after SCI in rats. Importantly, continuous infusion of the anti-Ryk antibody by osmotic minipumps resulted in the enhancement of the locomotor activity as well as the sprouting of the labeled CST. As our *in vitro* data demonstrate that neurite growth inhibition mediated by Wnt-5a is dependent on Rho-kinase, and that Wnt-5a activated RhoA in the CGNs, it is suggested that RhoA/Rho-kinase plays a role in the Wnt-mediated inhibition of axon growth *in vivo*.

Intracellular signals of axon growth inhibitors converge at RhoA and Rho-kinase

Several proteins in the CNS have been identified as inhibitors of axonal regeneration following the injury to the CNS in adult vertebrates. Three major inhibitors, Nogo, myelin-associated glycoprotein, and oligodendrocyte-myelin glycoprotein—expressed by oligodendrocytes and myelinated fiber tracts—have been identified (Yamashita et al., 2005). All these inhibitors were observed to bind to the Nogo receptor in complex with p75 or TROY, members of the TNF receptor family, and LINGO-1. The ligands binding to this receptor complex induce activation of RhoA and Rho-kinase and this signal transduction is necessary for axonal growth inhibition, at least *in vitro* (Mueller et al., 2005). Other studies have demonstrated that neurite outgrowth inhibitors, such as CSPG, and members of the semaphorin, ephrin, and repulsive guidance molecule families, also utilize the RhoA/Rho-kinase pathway for their inhibitory functions (Mueller et al., 2005). Our study demonstrates that the inhibitory effects of Wnt-5a depended on Rho-kinase *in vitro*, and that RhoA was activated in the CGNs when treated with Wnt-5a. Previous observations have demonstrated that these Wnts signal through RhoA and Rho-kinase. Activation of Rho-kinase by Wnt-3a induces neurite retraction from N1E-115 neuroblastoma cells (Kishida et al., 2004). Furthermore, a genetic study using zebrafish embryos demonstrated that the disruption of convergence and extension movement in *Wnt-5* or *Wnt-1* mutants was rescued by ectopic expression of RhoA or Rho-kinase, suggesting that RhoA/Rho-kinase act downstream of these Wnts (Zhu et al., 2005). Therefore, Wnt proteins expressed in cells surrounding the injured site may limit axon growth by activating RhoA/Rho-kinase in the neurons after SCI. Our findings suggest new candidates for the role of inhibitors of axon regeneration, which presumably employ common signaling.

Glial cells express axon growth inhibitors

In this study, we observed the induced expression of Wnt-5a in the reactive astrocytes surrounding the injury site

after SCI. CNS myelin derived from oligodendrocytes was first postulated as a major source of inhibition and several myelin-associated components that can inhibit axon outgrowth *in vitro* have been identified. In addition to the three above-mentioned myelin-derived inhibitors, the transmembrane semaphorin 4D (Moreau-Fauvarque et al., 2003), ephrin B3 (Benson et al., 2005), and repulsive guidance molecule (Hata et al., 2006) were proposed as members of the myelin-derived inhibitors. It is clear that CNS myelin exerts multiple layers of inhibitory influences *in vivo* as well as *in vitro* (Yamashita et al., 2005), although the extent of the relative contribution of each molecule remains to be determined. In addition to myelin, another important source of inhibition is the glial scar that forms after CNS injury. Many astrocytes in the injured area often become hypertrophic and adopt a reactive phenotype, releasing CSPG (McKeon et al., 1991). After injury, CSPG expression is rapidly up-regulated by reactive astrocytes, forming an inhibitory gradient that is highest at the center of the lesion. The intrathecal administration of chondroitinase ABC—an enzyme that removes GAG chains from the protein core—following SCI promoted the regeneration of various axon tracts as well as functional recovery (Bradbury et al., 2002; Moon et al., 2001). In addition, mutant mice that are deficient in both GFAP and vimentin exhibit reduced astroglial reactivity and this results in supraspinal sprouting and functional recovery after SCI (Menet et al., 2003), supporting the supposition that astrocytes may contribute to the inability of the injured spinal cord to regenerate. Therefore, our data, in combination with these findings, suggest that multiple inhibitors expressed in the reactive astrocytes, as well as myelin from the oligodendrocytes, may constitute a barrier that inhibits axon sprouting and functional recovery.

Multiple molecular targets for the treatment of SCI

Liu et al. (2008) reported that Wnt1 and Wnt5a were induced in the gray matter after unilateral hemisection of the spinal cord. Ryk was also induced in the CST axons. Injection of function blocking antibody to Ryk into the dorsal bilateral hemisectioned spinal cord prevented the retraction of CST axons or promoted growth of CST. Our results are consistent with these observations, although we have novel data, including *in vitro* experiments. Importantly, we observed improvement of the locomotor function after spinal contusion, which is more relevant to clinical conditiones, by the anti-Ryk antibody treatment. Although a growing number of candidate molecules are suggested to be implicated in the inhibition of the regeneration of injured CNS axons, the extent of the relative contribution of each molecule remains to be determined. Combination therapies designed to target multiple inhibitors may be more effective than those that target an individual component. As many of these inhibitors utilize common signals, such as RhoA/Rho-kinase, for axon growth inhibition, it may be postulated that the inhibition of RhoA or Rho-kinase would be one of the most effective approaches for the treatment of SCI patients. Indeed, the pharmacological inhibition of RhoA or Rho-kinase has been demonstrated to promote axon growth and locomotor activity (Dergham et al., 2002; Fournier et al., 2003; Hara et al., 2000; Sung et al., 2003; Tanaka et al., 2004). However, it should be noted that pharmacological inhibitors are not cell type specific and, therefore, act not only on neurons but also on other cell types, including astrocytes and oligodendrocytes. Anti-Ryk antibody treatment for the first 2 weeks was sufficient in our study, and this is the case for the Rho-kinase inhibitor treatment (Tanaka et al., 2004). Therefore, there seems to be some critical therapeutic period for the treatment of SCI. It is important to elucidate the whole network of the signal transduction mechanism of axon growth inhibition; therefore, our study provides evidence for a promising molecular target for the treatment of SCI.

Our observations strongly suggest that Wnt-Ryk signalling contributes significantly to the inability of the adult CNS to regenerate after injury. Although the CST axons are propelled down the spinal cord by a gradient of Wnt-1 and Wnt-5a acting through Ryk during the developmental stage, the severed CST axons in adults are stunted by the Wnt-Ryk signalling. The anti-Ryk antibody provides an effective therapeutic strategy for the treatment of CNS injury.

Acknowledgments

This work was supported by a Research Grant from National Institute of Biomedical Innovation (05–12) and Grant-in-Aid for Young Scientists (from JSPS to T.Y.).

Author Disclosure Statement

No competing financial interests exist.

References

Basso, D.M., Beattie, M.S., and Bresnahan, J.C. (1995). A sensitive and reliable locomotor rating scale for open field testing in rats. J. Neurotrauma 12, 1–21.

Benson, M.D., Romero, M.I., Lush, M.E., Lu, Q.R., Henkemeyer, M., and Parada, L.F. (2005). Ephrin-B3 is a myelin-based inhibitor of neurite outgrowth. Proc. Natl. Acad. Sci. USA 102, 10694–10699.

Bradbury, E.J., Moon, L.D., Popat, R.J., King, V.R., Bennett, G.S., Patel, P.N., Fawcett, J.W., and McMahon, S.B. (2002). Chondroitinase ABC promotes functional recovery after spinal cord injury. Nature 416, 636–640.

Ciani, L., and Salinas, P.C. (2005). WNTs in the vertebrate nervous system: from patterning to neuronal connectivity. Nat. Rev. Neurosci. 6, 351–362.

Dergham, P., Ellezam, B., Essagian, C., Avedissian, H., Lubell, W.D., and McKerracher, L. (2002). Rho signaling pathway targeted to promote spinal cord repair. J. Neurosci. 22, 6570–6577.

Fournier, A.E., Takizawa, B.T., and Strittmatter, S.M. (2003). Rho kinase inhibition enhances axonal regeneration in the injured CNS. J. Neurosci. 23, 1416–1423.

Hara, M., Takayasu, M., Watanabe, K., Noda, A., Takagi, T., Suzuki, Y., and Yoshida, J. (2000). Protein kinase inhibition by fasudil hydrochloride promotes neurological recovery after spinal cord injury in rats. J. Neurosurg. 93, 94–101.

Hata, K., Fujitani, M., Yasuda, Y., Doya, H., Saito, T., Yamagishi, S., Mueller, B.K., and Yamashita, T. (2006). RGMa inhibition promotes axonal growth and recovery after spinal cord injury. J. Cell Biol. 173, 47–58.

Kamitori, K., Machide, M., Osumi, N., and Kohsaka, S. (1999). Expression of receptor tyrosine kinase RYK in developing rat central nervous system. Brain Res. Dev. Brain Res. 114, 149–160.

Keeble, T.R., Halford, M.M., Seaman, C., Kee, N., Macheda, M., Anderson, R.B., Stacker, S.A., and Cooper, H.M. (2006). The Wnt receptor Ryk is required for Wnt-5a-mediated axon

guidance on the contralateral side of the corpus callosum. J. Neurosci. 26, 5840–5848.

Kishida, S., Yamamoto, H., and Kikuchi, A. (2004). Wnt-3a and Dvl induce neurite retraction by activating Rho-associated kinase. Mol. Cell Biol. 24, 4487–4501.

Kurayoshi, M., Oue, N., Yamamoto, H., Kishida, M., Inoue, A., Asahara, T., Yasui, W., and Kikuchi, A. (2006). Expression of Wnt-5a is correlated with aggressiveness of gastric cancer by stimulating cell migration and invasion. Cancer Res. 66, 10439–10448.

Liu, Y., Shi, J., Lu, C.C., Wang, Z.B., Lyuksyutova, A.I., Song, X.J., and Zou, Y. (2005). Ryk-mediated Wnt repulsion regulates posterior-directed growth of corticospinal tract. Nat. Neurosci. 8, 1151–1159.

Liu, Y., Wang, X., Lu, C.C., Kerman, R., Steward, O., Xu, X.M., and Zou, Y. (2008). Repulsive Wnt signaling inhibits axon regeneration after CNS injury. J. Neurosci. 28, 8376–8382.

Lu, W., Yamamoto, V., Ortega, B., and Baltimore, D. (2004). Mammalian Ryk is a Wnt coreceptor required for stimulation of neurite outgrowth. Cell 119, 97–108.

McKeon, R.J., Schreiber, R.C., Rudge, J.S., and Silver, J. (1991). Reduction of neurite outgrowth in a model of glial scarring following CNS injury is correlated with the expression of inhibitory molecules on reactive astrocytes. J. Neurosci. 11, 3398–3411.

Menet, V., Prieto, M., Privat, A., and Gimenez y Ribotta, M. (2003). Axonal plasticity and functional recovery after spinal cord injury in mice deficient in both glial fibrillary acidic protein and vimentin genes. Proc. Natl. Acad. Sci. USA 100, 8999–9004.

Moon, L.D., Asher, R.A., Rhodes, K.E., and Fawcett, J.W. (2001). Regeneration of CNS axons back to their target following treatment of adult rat brain with chondroitinase ABC. Nat. Neurosci. 4, 465–466.

Moreau-Fauvarque, C., Kumanogoh, A., Camand, E., Jaillard, C., Barbin, G., Boquet, I., Love, C., Jones, E.Y., Kikutani, H., Lubetzki, C., Dusart, I., and Chedotal, A. (2003). The transmembrane semaphorin Sema4D/CD100, an inhibitor of axonal growth, is expressed on oligodendrocytes and upregulated after CNS lesion. J. Neurosci. 23, 9229–9239.

Mueller, B.K., Mack, H., and Teusch, N. (2005). Rho kinase, a promising drug target for neurological disorders. Nat. Rev. Drug Discov. 4, 387–398.

Ren, X.D., Kiosses, W.B., and Schwartz, M.A. (1999). Regulation of the small GTP-binding protein Rho by cell adhesion and the cytoskeleton. Embo. J. 18, 578–585.

Schmitt, A.M., Shi, J., Wolf, A.M., Lu, C.C., King, L.A., and Zou, Y. (2006). Wnt-Ryk signalling mediates medial-lateral retinotectal topographic mapping. Nature 439,31–37.

Sung, J.K., Miao, L., Calvert, J.W., Huang, L., Louis Harkey, H., and Zhang, J.H. (2003). A possible role of RhoA/Rho-kinase in experimental spinal cord injury in rat. Brain Res. 959, 29–38.

Tanaka, H., Yamashita, T., Yachi, K., Fujiwara, T., Yoshikawa, H., and Tohyama, M. (2004). Cytoplasmic p21(Cip1/WAF1) enhances axonal regeneration and functional recovery after spinal cord injury in rats. Neuroscience 127, 155–164.

Uehata, M., Ishizaki, T., Satoh, H., Ono, T., Kawahara, T., Morishita, T., Tamakawa, H., Yamagami, K., Inui, J., Maekawa, M., and Narumiya, S. (1997). Calcium sensitization of smooth muscle mediated by a Rho-associated protein kinase in hypertension. Nature 389, 990–994.

Yamashita, T., Fujitani, M., Yamagishi, S., Hata, K., and Mimura, F. (2005). Multiple signals regulate axon regeneration through the Nogo receptor complex. Mol. Neurobiol. 32, 105–112.

Yoshikawa, S., McKinnon, R.D., Kokel, M., and Thomas, J.B. (2003). Wnt-mediated axon guidance via the Drosophila Derailed receptor. Nature 422, 583–588.

Zhu, S., Liu, L., Korzh, V., Gong, Z., and Low, B.C. (2005). RhoA acts downstream of Wnt5 and Wnt11 to regulate convergence and extension movements by involving effectors Rho kinase and Diaphanous: use of zebrafish as an in vivo model for GTPase signaling. Cell Signal. 18, 359–372.

Zou, Y. (2004). Wnt signaling in axon guidance. Trends. Neurosci. 27, 528–532.

Address reprint requests to:
Toshihide Yamashita, M.D., Ph.D.
Department of Molecular Neuroscience
Graduate School of Medicine
Osaka University
2-2 Yamadaoka, Suita
Osaka 565-0871, Japan

E-mail: yamashita@molneu.med.osaka-u.ac.jp

Cellular/Molecular

N-Acetylglucosamine 6-*O*-Sulfotransferase-1-Deficient Mice Show Better Functional Recovery after Spinal Cord Injury

Zenya Ito,[1,2] Kazuma Sakamoto,[1]* Shiro Imagama,[1,2]* Yukihiro Matsuyama,[2] Haoqian Zhang,[1] Kenichi Hirano,[2] Kei Ando,[2] Toshihide Yamashita,[3] Naoki Ishiguro,[2] and Kenji Kadomatsu[1,4]

Departments of [1]Biochemistry and [2]Orthopedics, Nagoya University Graduate School of Medicine, Nagoya 466-8550, Japan, [3]Department of Molecular Neuroscience, Graduate School of Medicine, Osaka University, Osaka 565-0871, Japan, and [4]Institute for Advanced Research, Nagoya University, Nagoya 464-8601, Japan

Neurons in the adult CNS do not spontaneously regenerate after injuries. The glycosaminoglycan keratan sulfate is induced after spinal cord injury, but its biological significance is not well understood. Here we investigated the role of keratan sulfate in functional recovery after spinal cord injury, using mice deficient in *N*-acetylglucosamine 6-*O*-sulfotransferase-1 that lack 5D4-reactive keratan sulfate in the CNS. We made contusion injuries at the 10th thoracic level. Expressions of *N*-acetylglucosamine 6-*O*-sulfotransferase-1 and keratan sulfate were induced after injury in wild-type mice, but not in the deficient mice. The wild-type and deficient mice showed similar degrees of chondroitin sulfate induction and of CD11b-positive inflammatory cell recruitment. However, motor function recovery, as assessed by the footfall test, footprint test, and Basso mouse scale locomotor scoring, was significantly better in the deficient mice. Moreover, the deficient mice showed a restoration of neuromuscular system function below the lesion after electrical stimulation at the occipito-cervical area. In addition, axonal regrowth of both the corticospinal and raphespinal tracts was promoted in the deficient mice. *In vitro* assays using primary cerebellar granule neurons demonstrated that keratan sulfate proteoglycans were required for the proteoglycan-mediated inhibition of neurite outgrowth. These data collectively indicate that keratan sulfate expression is closely associated with functional disturbance after spinal cord injury. *N*-acetylglucosamine 6-*O*-sulfotransferase-1-deficient mice are a good model to investigate the roles of keratan sulfate in the CNS.

Introduction

Neurons in the adult mammalian CNS do not spontaneously regenerate after injuries. Many factors contribute to this lack of repair, including a lack of growth-promoting factors (Widenfalk et al., 2001), the poor intrinsic regenerative capacity of CNS neurons (Neumann and Woolf, 1999), inhibitory factors associated with CNS myelin (Filbin, 2003; McGee and Strittmatter, 2003; Schwab, 2004), chemorepulsive molecules (De Winter et al., 2002), and glial scar-associated inhibitors such as chondroitin sulfate (CS) proteoglycans (CSPGs) (Silver and Miller, 2004).

The extracellular matrix of the adult CNS has a unique composition. Instead of collagens, laminin-1, and fibronectin, this matrix is rich in hyaluronic acid and CSPGs (Ruoslahti, 1996). CSPGs are reinduced after injury and inhibit neuronal axon regrowth. The inhibitory function of CSPGs on axonal outgrowth is primarily ascribed to their covalently attached CS-glycosaminoglycans, since the ablation of CS by use of chondroitinase ABC or a DNA enzyme that acts on xylosyltransferase enhances neuronal axon growth in CNS injury (Moon et al., 2001; Bradbury et al., 2002; Grimpe and Silver, 2004). For example, the axon growth of dopamine neurons is enhanced by chondroitinase ABC treatment after nigrostriatal tract transaction (Moon et al., 2001). Chondroitinase ABC treatment has been shown to enhance functional recovery after spinal cord injury in a rat model (Bradbury et al., 2002). It is known that CSPGs activate the Rho–Rho kinase pathway via an unknown receptor, leading to suppression of axonal growth (Borisoff et al., 2003; Mueller et al., 2005).

Keratan sulfate (KS) is another glycosaminoglycan. It is composed of repeating disaccharide units of galactose and *N*-acetylglucosamine (GlcNAc), where the C6 position of GlcNAc is always sulfated. The 5D4 antibody is commonly used for detection of KS, and it has been demonstrated that 5D4-reactive KS is induced in a rat model of spinal cord injury (Jones and Tuszynski, 2002). The reaction sequence for the biosynthesis of KS consists of *N*-acetylglucosaminylation, 6-sulfation of a GlcNAc residue exposed at the nonreducing end, and galactosylation (Habuchi et al., 2006; Kitayama et al., 2007). Because GlcNAc sulfation at the C6 position is necessary for KS chain elongation (Kitayama et al., 2007), failure of this sulfation leads to loss of KS synthesis. That is, deficiency of human *N*-acetylglucosamine 6-*O*-sulfotransferase-5 (GlcNAc6ST-5) leads to loss of corneal KS synthesis (Akama et al., 2000), and lack of mouse GlcNAc6ST-1 causes loss of 5D4-reactive KS expression in the CNS (Zhang et

Received June 2, 2009; revised Dec. 15, 2009; accepted March 8, 2010.

This work was supported in part by Ministry of Education, Culture, Sports, Science and Technology (MEXT) Grants-in-Aid 18390099 and 20390092 to K.K.; by funds from the 21st Century Centers of Excellence (COE) Program and Global COE Program of MEXT to Nagoya University; and by the Uehara Foundation. We thank T. Muramatsu (Aichi Gakuin University, Nagoya, Japan) for continuous support of this study.

*K.S. and S.I. contributed equally to this work.

Correspondence should be addressed to Kenji Kadomatsu, Department of Biochemistry, Nagoya University Graduate School of Medicine, 65 Tsurumai-cho, Aichi 466-8550, Japan. E-mail: kkadoma@med.nagoya-u.ac.jp.

DOI:10.1523/JNEUROSCI.2570-09.2010

 0270-6474/10/305937-11$15.00/0

al., 2006). In this study, to investigate the biological significance of KS in neurological function, we applied a contusion spinal cord injury model to *N*-acetylglucosamine 6-*O*-sulfotransferase-1-deficient mice and found that these mice showed better functional recovery than their wild-type counterparts.

Materials and Methods

Mice. GlcNAc6ST-1−/− mice were produced using D3 embryonic stem cells and an ordinary gene-targeting technology as described previously (Hemmerich et al., 2001). GlcNAc6ST-1+/− mice obtained after backcrossing with C57BL/6J for more than 11 generations were interbred. The littermates obtained were used for the spinal cord injury experiments. These mice were maintained in the animal facilities of Nagoya University. All experiments were performed in accordance with protocols approved by the institutional animal committee.

Spinal cord injury model. We anesthetized adult C57BL/6J mice, their wild-type littermates, and GlcNAc6ST-1−/− mice (female, 8 weeks old, 20–30 g) using an intraperitoneal injection of pentobarbital sodium (50 mg/kg). After laminectomy at the 10th thoracic spinal lamina, we exposed the dorsal surface of the dura mater. A bilateral contusion injury was created by delivering a 100 kdyn force to the cord using a commercially available spinal cord injury device (Infinite Horizon Impactor; Precision Systems and Instrumentation). Sham controls were subjected to laminectomy only. As postoperative care, the bladder was compressed by manual abdominal pressure twice per day until bladder function was restored, and prophylactic antibiotic treatment [1.0 ml of Bactramin (Roche) in 500 ml of acidified water] was maintained for 1 week. The numbers of mice used and mortality are summarized in supplemental Table 1 (available at www.jneurosci.org as supplemental material).

Reagents. Anti-KS 5D4 and anti-CS CS-56 monoclonal antibodies were purchased from Seikagaku. A biotin labeling kit-NH2 was used for biotinylation of the 5D4 antibody and purchased from Dojindo Molecular Technologies. CD11b monoclonal antibody was from BioLegend; Cy3-conjugated anti-glial fibrillary acidic protein (GFAP) monoclonal antibody was from Sigma; anti-Iba1 polyclonal rabbit antibody was from Wako; anti-platelet-derived growth factor receptor (PDGFr) polyclonal rabbit antibody was from Thermo Fisher Scientific Anatomical Pathology; anti-GAP-43 polyclonal rabbit antibody was from Millipore Bioscience Research Reagents; anti-serotonin (5HT) polyclonal rabbit antibody was from ImmunoStar; anti-type IV collagen polyclonal rabbit antibody was from LSL; and protein kinase Cγ was from Santa Cruz Biotechnology. Cy3- or Cy2-conjugated streptavidin and Cy3-conjugated anti-mouse IgM were from Jackson ImmunoResearch; Cy3-conjugated anti-rabbit IgG was from Zymed; and fluorescein isothiocyanate (FITC)-conjugated anti-rat IgG was from Sigma. FluorSave was obtained from Calbiochem.

Immunohistochemistry. Mice were perfused transcardially under deep ether anesthesia with buffered 4% paraformaldehyde. The spinal cords were removed, postfixed in 4% paraformaldehyde overnight, and cryoprotected in buffered 30% sucrose during the subsequent night. Tissues were cut into 12 μm sections with a cryostat and mounted on glass slides. Sections were blocked in PBS containing 3% bovine serum albumin (BSA) and 5% normal mouse serum for staining of biotin-conjugated anti-KS 5D4 or blocked in PBS containing 1% BSA and 10% normal goat serum for other immunohistochemistry. Sections were then incubated with the primary antibodies at 100× dilution in a blocking solution overnight at 4°C in PBS containing 3% BSA and 5% normal mouse serum or overnight at 4°C in 1% BSA and 10% normal goat serum. After rinsing in PBS, the sections were incubated with the secondary antibody (Cy3- or Cy2-conjugated streptavidin, 1:100; Cy3-conjugated goat anti-rabbit IgG, 1:100; Cy3-conjugated goat anti-mouse IgM, 1:100; or FITC-conjugated goat anti-rat IgG, 1:100) for 60 min at room temperature. Subsequently, the sections were rinsed in PBS, mounted with FluorSave, and examined by confocal microscopy (MRC 1024; Bio-Rad). GAP-43 staining was performed using 3,30-diaminobenzidine (Wako).

Anterograde labeling of the cortico-spinal tract. Eight weeks after injury, descending corticospinal tract (CST) fibers were labeled with biotin-dextran amine (BDA; 10% in saline; 3.2 μl per cortex; molecular weight, 10,000; Invitrogen) injected under anesthesia at the left and the right motor cortices (coordinates: 2 mm posterior to the bregma, 2 mm lateral to the bregma, 0.5 mm depth). For each injection, 0.2 μl of BDA was delivered for a period of 30 s via a 15–20-μm-inner-diameter glass capillary attached to a microliter syringe (ITO). Two weeks after BDA injection, the animals were killed by perfusion with PBS followed by 4% paraformaldehyde. The spinal cords were dissected, postfixed overnight in the same fixatives, and cryopreserved in 30% sucrose in PBS. A 20 mm length of spinal cord 10 mm rostral and 10 mm caudal to the lesion site was embedded in Tissue Tek OCT. These blocks were sectioned in the transverse plane (25 μm). Sections were blocked in PBS with 0.3% Triton X-100 for 4 h and incubated for 2 h with Alexa Fluor 488-conjugated streptavidin (1:400; Invitrogen) in PBS with 0.05% Tween 20. We then took serial cross sections of the spinal cord and performed quantitative analysis of the distribution of the axons. Degrees of BDA uptake were assessed by counting the total number of fibers in the cross section 5 mm rostral to the lesioned site, where the CST was intact. For quantification of the number of labeled corticospinal axons 5 mm caudal to the lesion site, the number of labeled fibers was counted in the gray matter and divided by the number of labeled corticospinal axons 10 mm above the lesion for each animal. The labeled fibers were counted using MetaMorph software. Light intensity and thresholding values were maintained at constant levels for all analyses.

Reverse transcription-PCR. The forward primer 5′-AAGCCTACAGGTGGTGCGAA-3′ and reverse primer 5′-CAGGACTGTTAACCCGCTCA-3′ were used for reverse transcription (RT)-PCR for GlcNAc6ST-1 expression, and the forward primer 5′-GGTGGAGGTCGGAGTCAACG-3′ and reverse primer 5′-CAAAGTTGTCATGGATGACC-3′ were used for RT-PCR for glyceraldehyde 3-phosphate dehydrogenase (GAPDH) expression. SuperScript III reverse transcriptase (Invitrogen) was used to synthesize cDNA.

Morphometry. The epicenter of a lesion was determined by hematoxylin and eosin staining of several of the serial 12 μm sections. All the image analyses were performed using spinal cord samples prepared from six sagittal sections at 12 μm intervals (three sections on either side of the midline, which was identified by the appearance of the central tube), and all the axial image analyses in Figure 6 were performed using spinal cord samples from positions 5 mm caudal to the lesion site. Statistical analyses were performed for five mice for each experimental group. To count reactive astrocytes, standardized areas for sampling in six sections from each animal in each group were identified as a 600-μm-wide band of spinal cord adjoining the cord–lesion interface in each section.

Mean values for each animal were then compared. Light intensity and thresholding values were maintained at constant levels for all analyses by a computer-driven microscope stage (MetaMorph Offline version 6.3 r^2; Molecular Devices). The amounts of fibrous tissue and axonal outgrowth of the wound area were assessed by counting signals visualized by staining with anti-type IV collagen, CD11b, CS-56, GAP-43, and 5HT antibodies, respectively, for 640 × 2200 μm^2 counting frames around a lesion. Data were collected for at least five mice with each genotype in each experiment.

Footfall test. Mice were subjected to the grid runway test to assess locomotor function recovery at 6 weeks after injury. Performance on a wire grid was evaluated for 3 min by counting footfalls. A footfall was defined as either hindpaw missing a rung and extending through the space between adjacent grids. The wire grid was positioned flat and was 7 × 11 inches with grid squares of 0.35 × 0.35 inches. The number of footfalls was counted for five mice in each group.

Footprint test. In the footprint analysis, the hindpaws were covered with ink to record walking patterns during continuous locomotion across a paper runway (1.2 × 12 inches) at 6 weeks after injury, and the stride lengths were calculated. Strides were analyzed only when mice ran with constant velocity. All strides on the first and last 5 cm of the passage were excluded because of changing velocity.

Behavioral testing. The locomotor performance of animals was analyzed using the Basso mouse scale (BMS) open-field score (Basso et al., 2006) for 8 weeks, since the BMS has been shown to be a valid locomotor rating scale for mice. The evaluations were made by two blind observers for all analyzed groups. Briefly, the BMS is a nine-point scale that pro-

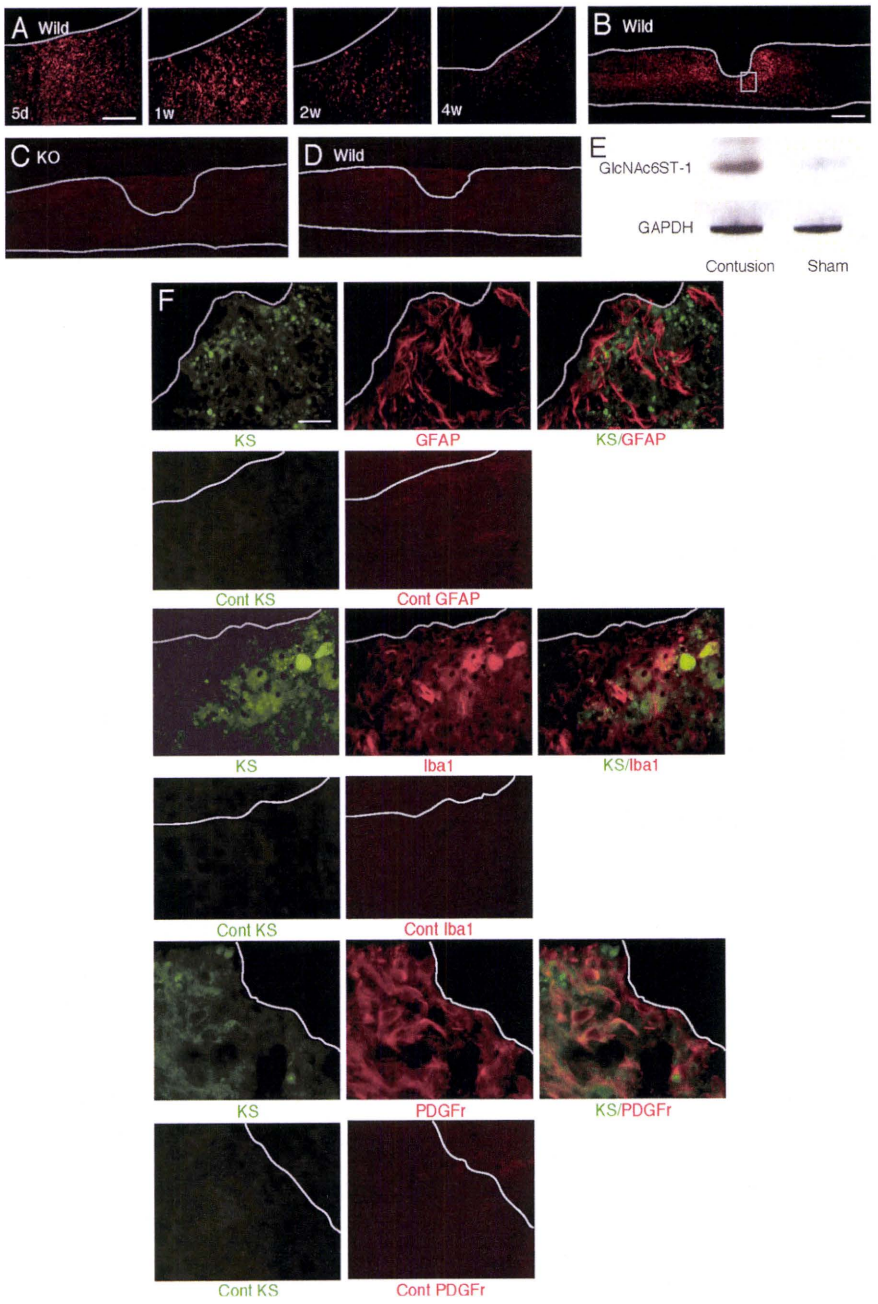

Figure 1. KS expression after spinal cord injury. ***A***, Expression profile of 5D4-reactive KS in wild-type mice after spinal cord injury. Scale bar, 100 μm. d, Day; w, week. ***B–D***, KS was expressed around the lesion center 7 d after injury in wild-type mice (***B***) but was not detected in GlcNAc6ST-1−/− mice (KO; ***C***) or isotype-matched IgG controls (***D***). ***E***, RT-PCR for GlcNAc6ST-1 and GAPDH was performed for samples from the wild-type mouse spinal cord 7 d after injury or sham operation. ***F***, Double staining for KS and a glial cell marker. Reactive astrocytes (GFAP), microglia (Iba1), and oligodendrocyte precursors (PDGF receptors) were examined. Scale bar, 50 μm. The sections shown are midline sagittal sections of the injured spinal cord. The drawn lines indicate the margins of the lesion core (***A***) and the outline of the spinal cord (***B***, ***C***).

vides a gross indication of locomotor ability and determines the phases of locomotor recovery and features of locomotion. The BMS score was determined for seven mice in each group.

Electrophysiology. In terminal electrophysiological experiments, after an intraperitoneal injection of ketamine (100 mg/kg), short trains of five square-wave stimuli of 0.5 ms duration with an interstimulus interval of 2 ms were delivered through the occipito-cervical area by small electrode balls, and needle electrodes were placed in both hindlimbs. The active electrode was placed in the muscle belly, and the reference electrode was placed near the distal tendon of the muscle in each limb. The ground electrode was placed subcutaneously between the coil and the recording electrodes. The onset latency was measured as the length of time in milliseconds between the stimulus and the onset of the first wave. One hundred responses were averaged and stored for off-line analysis of latency.

Cell culture. Sprague Dawley rats at postnatal days 7–9 were killed, and the cerebella were collected. The meninges were carefully removed with fine forceps, and the remaining tissues were minced and digested using a Papain Dissociation System (Worthington). Dissociated cells were applied to a 35/60% two-step Percoll gradient and centrifuged at 3000 × *g* for 15 min. Cerebellar granule neurons at the interface were collected. Cells were suspended in Neurobasal medium (Invitrogen) supplemented with 2% B27 (Invitrogen), 2 mM glutamine, an additional 20 mM KCl, 50 U/ml penicillin, and 50 μg/ml streptomycin.

Substrate preparation. Four-well chamber slides (NUNC) were coated with 20 μg/ml poly-L-lysine (PLL; Sigma) and left overnight at 4°C and then were coated with chick brain proteoglycans (Millipore Bioscience Research Reagents) or the other indicated substrates and left for 4 h at 37°C. If indicated, proteoglycans were treated with 200 mU/ml chondroitinase ABC or 5 mU/ml keratanase II derived from *Bacillus* sp. Ks36 (Seikagaku) in PBS at 37°C. Other substrate materials included poly-L-ornithine, myelin-associated glycoprotein (Sigma), Nogo, oligodendrocyte myelin glycoprotein (R & D Systems), KS and chondroitin sulfate C (Seikagaku).

Cell adhesion assay. Cerebellar granule neurons were seeded onto chick proteoglycan-coated chamber slides at 2.0×10^5 per well. After 2 h, nonadherent cells were washed out with PBS, and adherent cells were visualized by nuclear staining with 4′,6-diamidino-2-phenylindole (DAPI). The number of adherent cells was counted under 200× magnification (six fields).

Neurite outgrowth assays. Cerebellar granule neurons were seeded onto four-well chamber slides at 2.0×10^5 per well. Twenty-four hours after seeding, the neurons were fixed with 4% paraformaldehyde/PBS and stained with anti-neuron-specific β-tubulin (Covance) to visualize neurites. Neurite lengths were measured from at least 100 neurons that had neurites longer than twice the cell body diameter, per condition from duplicate wells, and quantified as described previously (Ughrin et al., 2003).

Isolation and purification of proteoglycans from mouse brains. Whole brains were isolated from C57BL/6J mice (postnatal day 5). Tissues were homogenized in PBS containing 10 mM *N*-ethylmaleimide and protease inhibitor mixtures (Nacalai Tesque) using a Dounce-type homogenizer. Homogenates were centrifuged at 24,000 × *g* for 30 min, and supernatants were applied to DEAE-Sepharose (GE Healthcare). Samples were washed three times with wash buffer (50 mM Tris-HCl, pH 7.5, 2 M urea, 0.25 M NaCl, 20 mM EDTA, 0.2 mM PMSF, 1 mM *N*-ethylmaleimide), and the proteoglycans were eluted with 2 M NaCl. The eluent was concentrated using a size-exclusion spin column (molecular weight cutoff, 100 kDa), and the protein concentration was determined using a Micro BCA Protein Assay kit (Thermo Fisher Scientific).

Spot assay. PLL-coated chamber slides were air dried and spotted with 5 μl of proteoglycans (10 μg/ml) from mouse brains. The spotted area was visualized by staining with rhodamine B (10 μg/ml). If indicated, proteoglycans were predigested with keratanase (500 mU/ml) and keratanase II (5 mU/ml) at 37°C for 2 h before spotting. Cerebellar granule neurons were seeded onto four-well chamber slides at 1.0×10^5 or 1.0×10^6 per well.

Coating efficiency. Five microliters of aggrecan (50 μg/ml), which had been treated with or without keratanase (500 mU/ml) and keratanase II (5 mU/ml) at 37°C for 2 h, were spotted onto PLL-coated chamber slides. After overnight incubation at 37°C, the coated aggrecan was visualized using an anti-CS antibody (CS56), followed by Alexa-488-conjugated anti-mouse IgM antibody.

Statistical analysis. Statistical analyses were performed with an unpaired two-tailed Student's *t* test for single comparisons and one-way ANOVA for multiple comparisons. For the footfall and footprint scores, repeated-measures ANOVA and the Mann–Whitney *U* test were used. In all statistical analyses, values of $p < 0.05$ were considered to indicate significance. To obtain the data for statistical analyses, the investigators were blinded to the genotypes in all procedures.

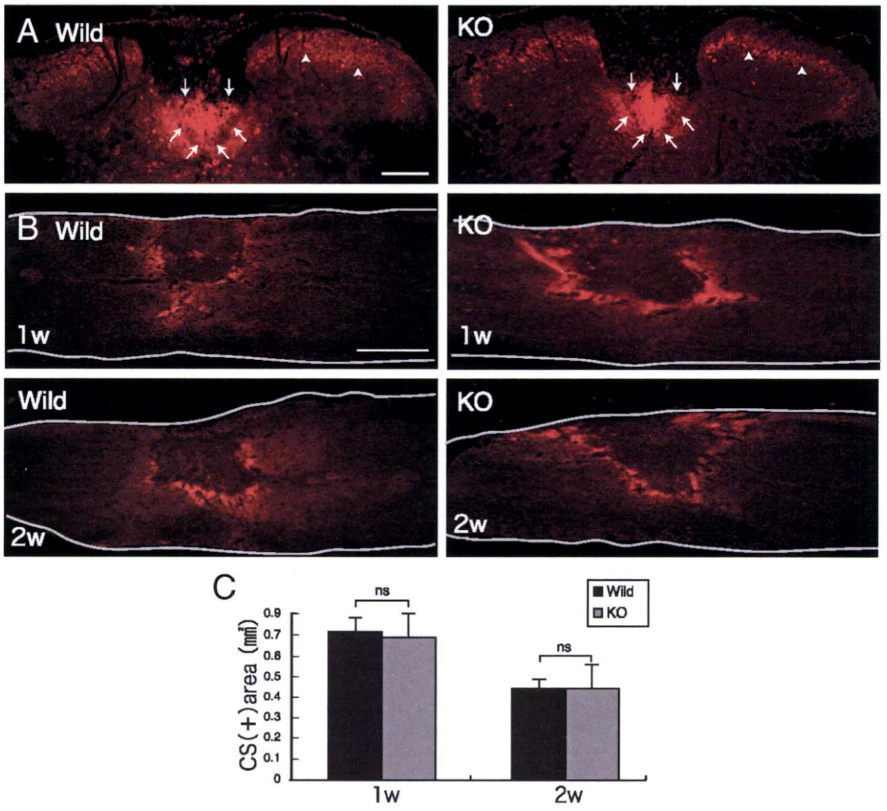

Figure 2. CST and CS expression after injury. ***A***, The CST was stained with anti-protein kinase C-γ antibody (arrow). Densely packed immunofluorescent small cells are located in the inner part of lamina II of the substantia geratinosa (arrowhead) on the axial section. Scale bar, 200 μm. The sections shown are axial sections of the injured spinal cord. ***B***, CS expression was determined with CS-56 antibody. Scale bar, 500 μm. The sections shown are the midline sagittal sections of the injured spinal cord. The drawn lines indicate the outline of the spinal cord. ***C***, Quantification of CS expression. Five mice for each genotype at each time point were examined. Quantification data are the means ± SEM. ns, Not significant (Student's *t* test). w, Week; KO, knock-out.

Results

Induction of KS expression after spinal cord injury in wild-type mice

We used a contusion injury model of the spinal cord to investigate the significance of KS in neurological function after injuries. The contusion injury of the spinal cord was made at the 10th thoracic level with 100 kdyn using an Infinite Horizon Impactor. To reveal the expression and localization of KS, 5D4, an anti-KS monoclonal antibody, was used. 5D4-reactive KS expression was induced around the core lesion, reached a maximum level around 5–7 d after injury in wild-type mice (Fig. 1*A*), and was not detected at all in GlcNAc6ST-1−/− mice (Fig. 1*B–D*). GlcNAc6ST-1 expression was also enhanced in injured wild-type mice (Fig. 1*E*).

Antibodies against GFAP, Iba1, and PDGFr were used to identify KS-expressing cells. 5D4-reactive KS did not overlap GFAP, but a portion of the Iba1-positive cells overlapped 5D4-reactive cells (Fig. 1*F*). Almost all PDGFr-positive cells were 5D4 positive (Fig. 1*F*). These data indicated that KS was mainly expressed by oligodendrocyte precursor cells (PDGFr positive) and partially expressed by microglia (Iba1 positive), which is consistent with the 5D4-reactive KS expression previously reported in a rat spinal cord injury model (Jones and Tuszynski, 2002).

CST, CS expression, and inflammatory cell accumulation

Protein kinase C-γ is a marker for the CST. Protein kinase C-γ immunoreactivity was observed in the dorsal column and lamina II of the spinal cords of uninjured mice (Fig. 2*A*, arrows and arrowheads, respectively) at the T5 level of the cord. The immunoreactivity was similar in wild-type and GlcNAc6ST-1−/− mice (Fig. 2*A*), and the BMS locomotor score before spinal cord injury was also similar in both groups (data not shown), indicating that the CST had formed in a normal fashion in GlcNAc6ST-1−/− mice and thus that these mice could be used for the motor function analyses.

In contrast to KS expression, CS expression in GlcNAc6ST-1−/− mice as judged by CS-56 immunoreactivity was comparable to that in wild-type mice (Fig. 2*B*, *C*). Furthermore, CD11b (a marker of monocytes/macrophages and granulocytes)-positive inflammatory cells were accumulated in the lesion to a similar extent in wild-type and GlcNAc6ST-1−/− mice (data not shown).

Motor function

We next evaluated functional recovery after injury. The footfall test and footprint test were used to objectively evaluate motor function. For the footfall test, mice were placed on a lattice of thin metal wires. This test requires accurate limb placement and precise motor control. Intact animals cross the grid without making footfalls, whereas a paralytic foot tends to fall from the lattice during movement. The numbers of footfalls were comparable between wild-type and GlcNAc6ST-1−/− mice 3 d after injury (Fig. 3*A*). GlcNAc6ST-1−/− mice gradually recovered and, at 4–6 weeks after injury, showed footfall counts comparable to those of sham-operated mice (Fig. 3*A*). In contrast, wild-type mice still showed frequent footfalls at 4 and 6 weeks after injury (Fig. 3*A*; see movie in supplemental Fig. S1, available at www.jneurosci.org as supplemental material).

On the footprint test, GlcNAc6ST-1−/− mice showed a well balanced and organized walk at 4 weeks after injury, whereas wild-type mice showed a disorganized walk, sometimes with toe drop (Fig. 3*B*, arrow). The profiles of stride length deduced

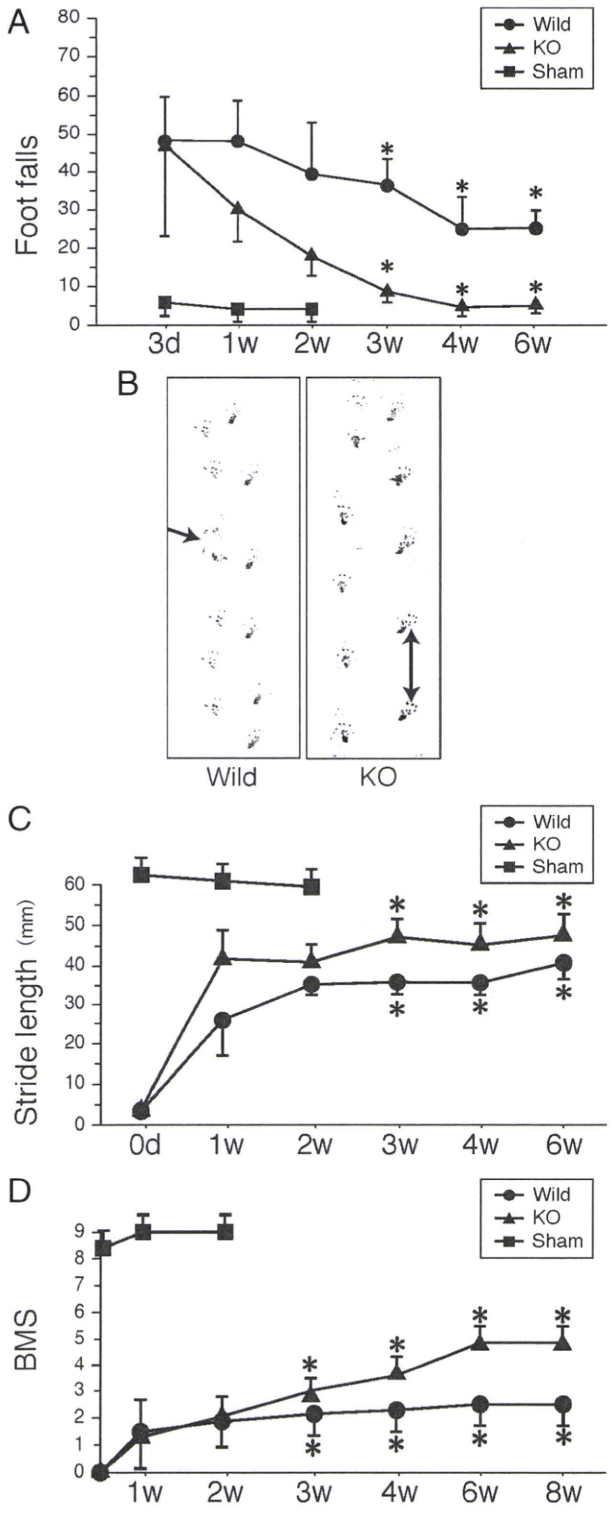

Figure 3. Footfall and footprint tests and BMS scoring. ***A***, Footfall test. The graph shows data from five mice for each genotype at each time point. ***B***, Representative photos of the footprint test taken 4 weeks after injury. The arrow indicates a toe drop. ***C***, Data of the footprint test are quantified. Five mice were used for each genotype at each time point. Quantification data are the means ± SEM (repeated-measures ANOVA and the Mann–Whitney *U* test). ***D***, BMS scoring. The graph shows data from seven mice for each genotype at each time point. $*p < 0.05$ (wild-type vs GlcNAc6ST-1−/− mice). d, Day; w, week; KO, knock-out.

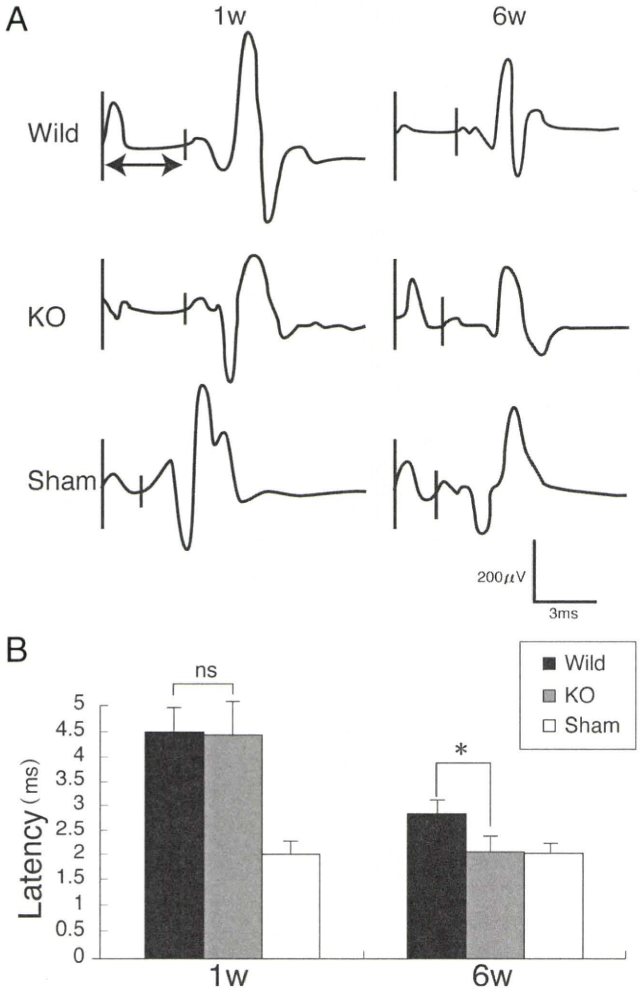

Figure 4. Motor-evoked potential. ***A***, Representative profiles of motor-evoked potentials are shown. ***B***, Latency times were quantified. Five mice were used for each genotype at each time point. $*p < 0.05$. Quantification data are the means ± SEM (one-way ANOVA). W, week; KO, knock-out; ns, not significant.

from the footprints clearly demonstrated that the recovery of motor function was significantly better in GlcNAc6ST-1−/− mice (Fig. 3*C*).

We also performed BMS locomotor scoring for 8 weeks. There was a significantly better recovery in the GlcNAc6ST-1−/− mice than in the wild-type controls (Fig. 3*D*). These data were consistent with those of our footfall scoring and footprints, in which a significant recovery was observed from 3 weeks after the spinal cord injury (Fig. 3*B–D*). Using the same mice as used for BMS scoring, we also examined the footfall test results over a longer period (supplemental Fig. S2 and Table 1, available at www.jneurosci.org as supplemental material) and confirmed the reproducibility of the data in Figure 3*A*. These mice were also compared with hemisection and total section models as described below.

Next, to confirm that our 100 kdyn contusion model inflicted an injury of sufficient severity, we subjected additional mice to total section and hemisection injuries and compared their motor function with that of our 100 kdyn contusion injury model. In the footfall test, the hemisection model showed a substantial degree of spontaneous recovery, reaching an almost normal level 6 weeks after spinal cord injury, whereas the total section model showed a severe motor function disturbance even 6 weeks after injury. The 100 kdyn contusion injury was more severe than the

hemisection injury but milder than the total section injury (supplemental Fig. S2, available at www.jneurosci.org as supplemental material). Furthermore, in the BMS scores of wild-type mice, we did not observe spontaneous recovery of motor function even 8 weeks after contusion injury (Fig. 3*D*). Together, these results suggest that our contusion model was sufficiently severe and was appropriate for evaluating functional recovery after spinal cord injury.

Motor-evoked potential has been widely used in clinical and animal trials of spinal cord injury to evaluate the neuromuscular system function. In the present work, the latency of motor-evoked potential was measured to also objectively evaluate motor function. Mice received electrical stimuli at the occipito-cervical area, and the motor-evoked potential was recorded at both hindlimbs. The latency of the motor-evoked potential was measured from the onset of the stimulus to the first response of each wave. At 1 week after injury, the latency was elongated to a similar extent in wild-type and GlcNAc6ST-1−/− mice, but at 6 weeks after injury, the latency of GlcNAc6ST-1−/− mice became comparable to that of the sham-operated controls, whereas that of wild-type mice was significantly longer (Fig. 4). These data support the conclusion that functional recovery was significantly better in GlcNAc6ST-1−/− mice.

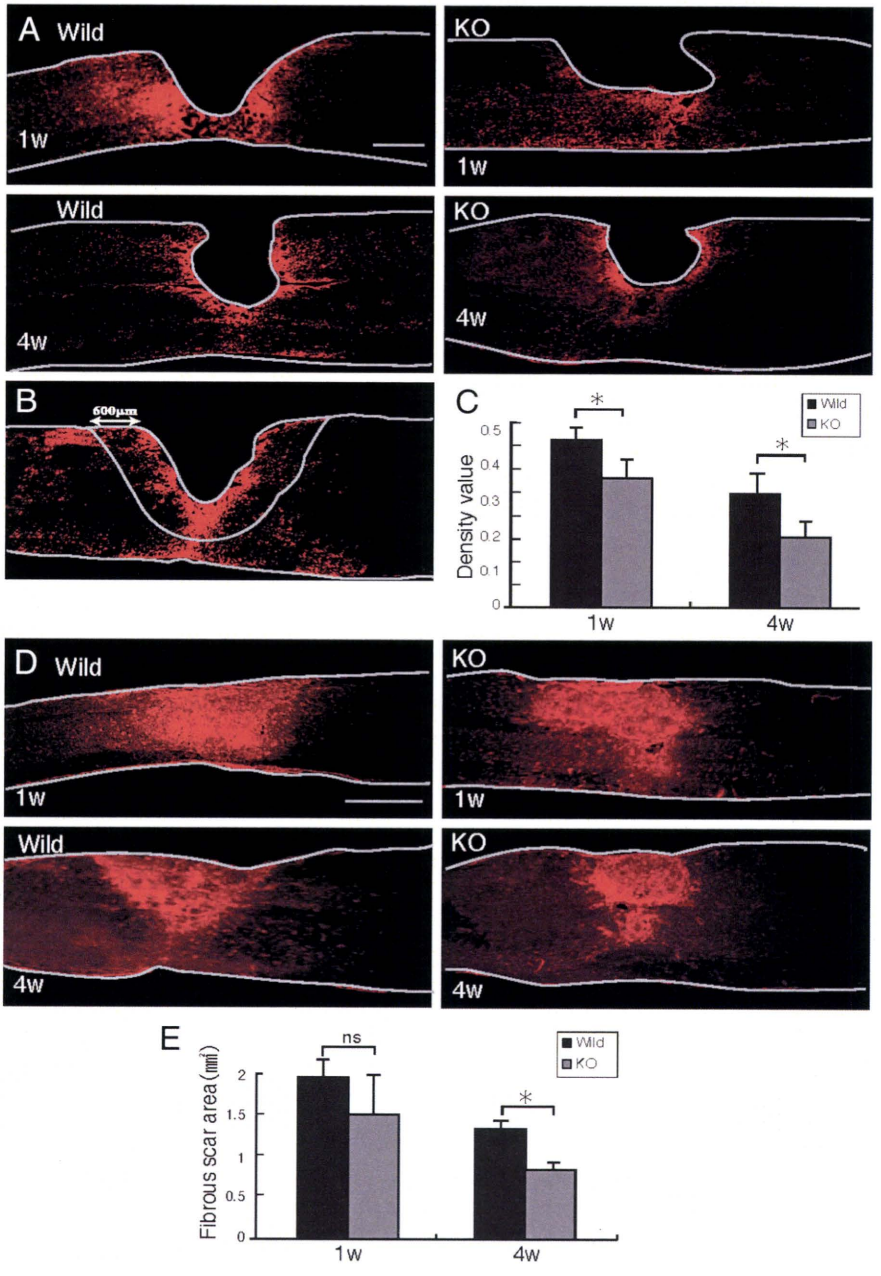

Figure 5. Reactive astrocyte accumulation and collagen IV deposition. ***A***, Representative photos for GFAP expression are shown. Scale bar, 500 μm. The drawn lines indicate the margins of the lesion core and the outline of the spinal cord. ***B***, The GFAP-positive area in a field of 600 μm width around the lesion center (lack of GFAP signal) was measured. The drawn lines indicate the outline of the spinal cord and the measured area. ***C***, The GFAP-positive area is summarized in the graph. Five mice were used for each genotype at each time point. $*p < 0.05$. ***D***, Representative photos for collagen IV expression are shown. Scale bar, 500 μm. The drawn lines indicate the outline of the spinal cord. ***E***, The collagen IV-positive areas are summarized in the graph. Five mice were used for each genotype at each time point. $*p < 0.05$. Quantification data are the means ± SEM (Student's *t* test). The sections shown are midline sagittal sections of the injured spinal cord. W, week; KO, knock-out; ns, not significant.

Glial scar formation

We next examined glial scar formation. Accumulation of GFAP-positive reactive astrocytes appeared after injury in both wild-type and GlcNAc6ST-1−/− mice. However, their accumulation was weaker in GlcNAc6ST-1−/− mice than in wild-type mice: the GFAP-positive area in a region of 600 μm width around the lesion core was significantly smaller in GlcNAc6ST-1−/− mice (Fig. 5*A–C*). An important marker for glial scarring is collagen IV, which appears in the late stages of glial scarring (Liesi and Kauppila, 2002). In the present study, collagen IV expression in the injured area became apparent 7 d after injury in both wild-type and GlcNAc6ST-1−/− mice, but the margin was unclear. There was no difference in scar area (the collagen IV-positive area) between the two genotypes. The margin of the scar area became clear at 4 weeks after injury, and the scar area was significantly reduced in GlcNAc6ST-1−/− mice (Fig. 5*D*,*E*).

Neuronal axon growth

Regeneration of the serotonergic descending raphespinal tract may partly explain the reason for motor function recovery after spinal cord injury in rodents (Kim et al., 2004). We stained tissues 5 mm distal to the lesion for 5-hydroxytryptamine (5HT), since serotonergic axons are 5HT positive. 5HT-positive fibers were more abundantly found in the ventral horn of the gray matter in GlcNAc6ST-1−/− mice than in wild-type mice (5HT-positive area: wild-type, 972 ± 1080 vs GlcNAc6ST-1−/−, 7120 ± 1168 μm^2; $p < 0.005$) (Fig. 6*A–C*). Positive GAP-43 staining reflects axon regeneration and sprouting (Tetzlaff and Bisby, 1989; King et al., 2001). GAP-43-positive axons were also much more abun-

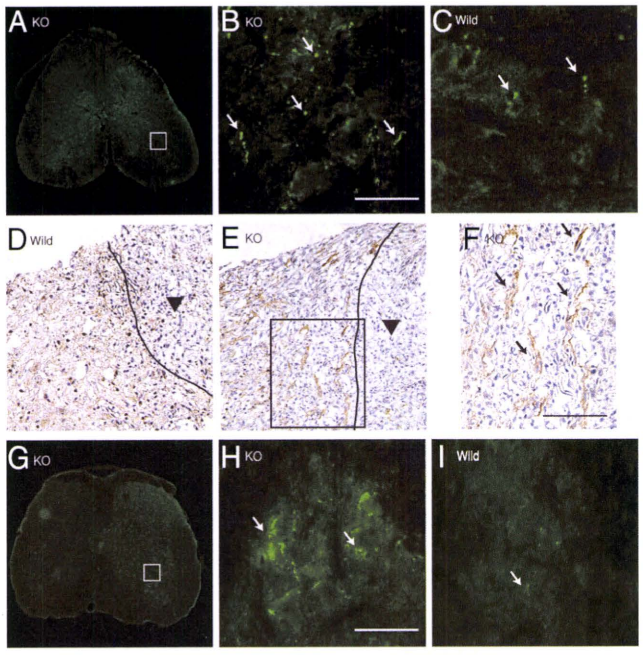

Figure 6. Axonal growth. 5HT staining of the ventral horn (***A–C***; 5 mm distal to the lesion), GAP43 staining (***D–F***), and tracer-fiber counts of the CST (BDA-positive fibers) (***G–I***; 5 mm caudal to the lesion) are shown for GlcNAc6ST-1−/− (***A***, ***B***, ***E–H***) and wild-type (***C***, ***D***, ***I***) mice. Scale bar, 50 μm. Higher-magnification figures of the boxed areas in ***A***, ***E***, and ***G*** are shown in ***B***, ***F***, and ***H***, respectively. The arrows in ***B***, ***C***, ***F***, ***H***, and ***I*** indicate 5HT-, GAP43-, and BDA-positive fibers, respectively. The arrowheads in ***D*** and ***E*** indicate the contusion area. The drawn lines indicate the margins of the lesion core. Five mice were used for each genotype at 4 weeks after injury. The sections in ***A–C***, ***G***, ***H***, and ***I*** are the axial sections of the injured spinal cord. The sections in ***D–F*** are the midline sagittal sections of the injured spinal cord. KO, Knock-out.

dant in GlcNAc6ST-1−/− mice than in wild-type mice at 4 weeks after injury (GAP-43-positive fiber counts/150,000 μm^2: wild-type, 1962 ± 1522 vs GlcNAc6ST-1−/−, 6631 ± 1090; $p < 0.005$) (Fig. 6*D–F*). Moreover, we investigated axonal growth in the CST. In tracer-fiber counts for the CST, the number of BDA-positive fibers was increased in the region caudal to the epicenter in GlcNAc6ST-1−/− mice, particularly in the gray matter in this region (Fig. 6*G–I*). For quantification of the number of labeled BDA, the number of labeled fibers was counted in the gray matter 5 mm caudal to the lesion and divided by the number of labeled corticospinal axons 10 mm rostral to the lesion for each animal. There was a significant difference between wild-type and GlcNAc6ST-1−/− mice (BDA-positive fibers in caudal region/rostral region: wild-type, 1.9 ± 1.1% vs GlcNAc6ST-1−/−, 6.9 ± 1.0%; $p < 0.005$).

Chondroitinase ABC promotes collateral sprouting of spared fibers in the cuneate nucleus after cervical spinal cord injury (Massey et al., 2006), suggesting that proteoglycans limit not only axon regeneration but also sprouting. Our data on 5HT staining, GAP-43 staining, and CST tracer-fiber counts are in line with this idea.

Requirement of KS for the proteoglycan-mediated inhibition of neurite growth

To further explore the underlying mechanisms involving KS in the functional disturbance, we performed *in vitro* experiments. We first asked whether KS was sufficient to inhibit neurite growth. However, glycosaminoglycans (KS and CS), whether administered singly or in combination, did not inhibit neurite outgrowth (Fig. 7*A*). Thus, we focused on the role of KS chains on proteoglycans.

Proteoglycans purified from the brains of chicks contained both KS and CS, because the 5D4-reactive smear appeared more strongly after the CS-degrading enzyme chondroitinase ABC treatment, and the smear disappeared after keratanase II treatment on Western blot analysis (Fig. 7*B*). As it is known that proteoglycans inhibit not only neurite outgrowth but also cell adhesion to the substrate (Kaneko et al., 2007), we examined whether the proteoglycans used in this study would inhibit cell–substrate adhesion. As shown in Figure 7, *C* and *D*, the number of cells adhered to the substrate decreased as the concentration of coated proteoglycans increased. However, if the proteoglycan concentration was lower than 300 ng/ml, the number of cells adhering to the proteoglycans was comparable to the number adhering to the PLL-coated slides (Fig. 7*C*,*D*). Therefore, we decided to use the condition of 300 ng/ml proteoglycans for coating in the neurite outgrowth assay, so that we could discriminate the effect of proteoglycans on neurite outgrowth from that on cell–substrate adhesion.

Proteoglycans coated on the substratum strikingly inhibited the neurite outgrowth of primary neurons compared with the PLL control (Fig. 7*E*,*F*). Molecules derived from myelin, such as Nogo, myelin-associated glycoprotein, and oligodendrocyte-myelin glycoprotein, are known as strong *in vivo* inhibitors of axonal regrowth. Our *in vitro* assay showed that these molecules also inhibit the neurite outgrowth of primary granular neurons from the rat cerebellum (Fig. 7*F*). Notably, the KS-degrading enzyme keratanase II blocked the proteoglycan-mediated inhibition, and this blocking effect was comparable to that of chondroitinase ABC (Fig. 7*E*,*F*).

Finally, we developed an assay system, the spot assay, and used it to examine the activity of mouse brain proteoglycans. We first confirmed that the mouse brain proteoglycans indeed contained both KS and CS (Fig. 8*A*). We then spotted these proteoglycans with rhodamine B, so that the spots appeared red (Fig. 8*B*). Whereas neurites of the primary neurons frequently crossed into the spots in the control (rhodamine B alone) (Fig. 8*B*, top), neurites of neurons in the surrounding area did not enter into the spots of the mouse brain proteoglycans (Fig. 8*B*, middle). However, if the proteoglycans were treated with keratanase, neurites of neurons in the surrounding area could enter the spots (Fig. 8*B*, bottom). This phenomenon was more clearly demonstrated if the seeded cell number was decreased (Fig. 8*C*). Therefore, this *in vitro* assay using brain proteoglycans mimicked the *in vivo* failure of axonal regrowth into the lesions of spinal cord injury and the reversal of this failure in KS-deficient mice.

To examine the possibility that keratanase decreases the efficiency of proteoglycan binding to the substrate, we used the KS/CSPG aggrecan for spotting and visualized spots with the anti-CS antibody CS56. However, we did not observe any difference between spots with and without predigestion with keratanase (supplemental Fig. S3, available at www.jneurosci.org as supplemental material).

Discussion

There have been only a few studies on the relationship between KS and the nervous system. KS expression is induced in the injured CNS after cortical stab wounds in neonatal rats and in the postcomissural fornix after lesioning in adult rats (Geisert and Bidanset, 1993; Stichel et al., 1999). KS expression is also enhanced in reactive microglia and oligodendrocyte progenitors after rat spinal cord injury (Jones and Tuszynski, 2002). After

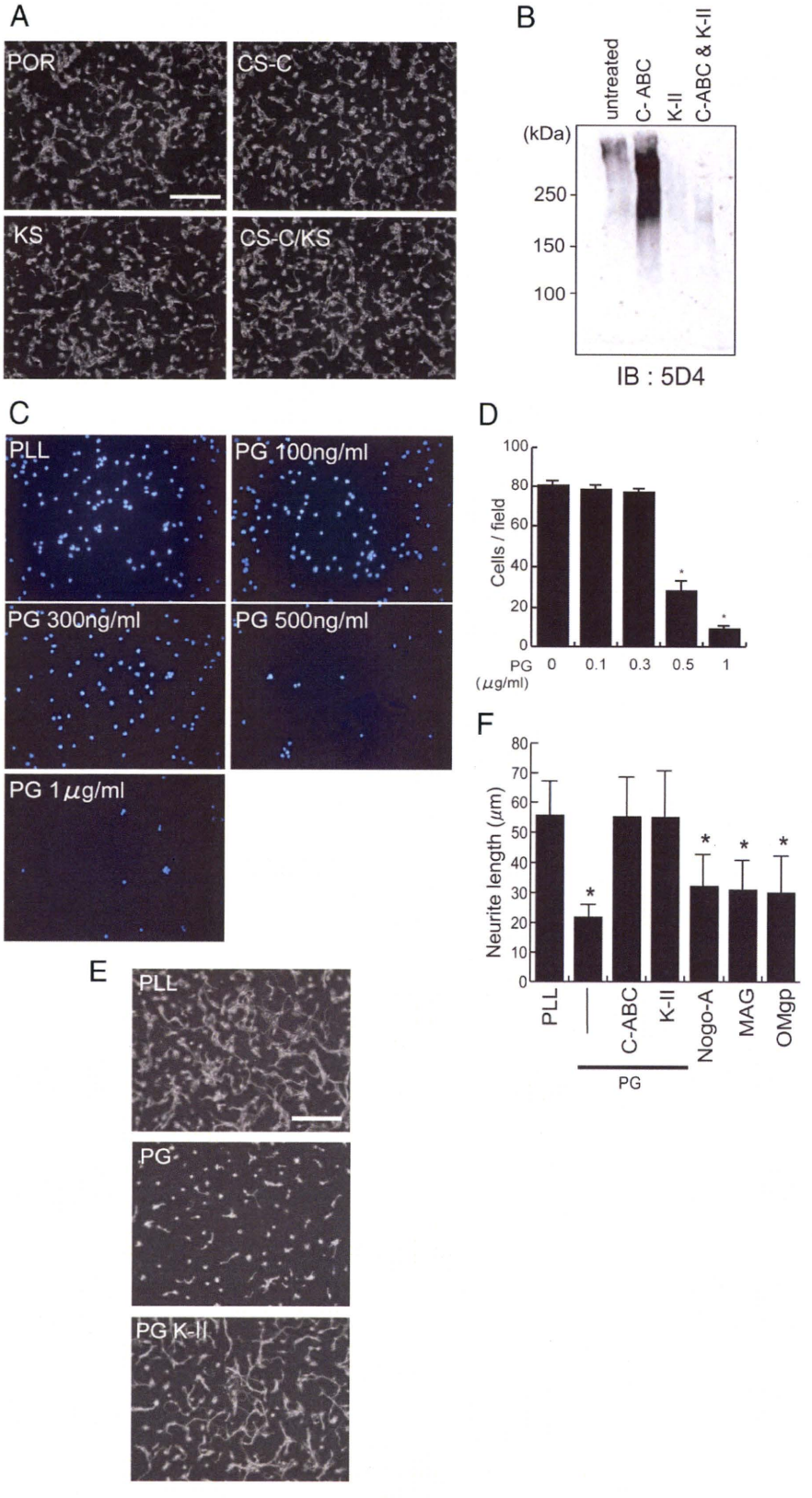

Figure 7. Requirement of KS for the proteoglycan-mediated inhibition of neurite outgrowth. ***A***, Postnatal day 8 (P8) rat cerebellar granule neurons were cultured on poly-L-ornithine (POR), POR plus chondroitin sulfate C (CS-C) (20 μg/ml), or POR plus KS (20 μg/ml). Scale bar, 100 μm. ***B***, Chick brain proteoglycans contained KS. Chick brain proteoglycans (CC117; Millipore) were digested with chondroitinase ABC (C-ABC; 500 mU/ml), keratanase II (K-II; 5 mU/ml), or both and subjected to Western blot analysis. Note that C-ABC treatment revealed KS epitopes. ***C***, P8 rat cerebellar granular neurons were cultured on PLL or proteoglycan (PG) extracted from chick brains. To count adhered cells, the nucleus was stained with DAPI, and the cell number was counted for six fields under 200× magnification. ***D***, The quantification of ***C***. Data represent the average cell number ± SD. *$p <$ 0.01, versus 0 μg of PG. ***E***, P8 rat cerebellar granular neurons were cultured on PLL or PG extracted from chick brains. Keratanase II treatment restored the neurite outgrowth. Scale bar, 100 μm. ***F***, The quantification of ***E***. Data represent the average neurite length ± SD. *$p < 0.05$ versus PLL. PG (300 ng/ml), C-ABC (200 mU/ml), K-II (5 mU/ml), Nogo (800 ng/ml), myelin-associated glycoprotein (MAG) (400 ng/ml), and oligodendrocyte myelin glycoprotein (OMgp) (400 ng/ml) were used.

unilateral axotomy of the nigrostriatal tract in adult rats, CSPGs and keratan sulfate proteoglycans (KSPGs) are predominantly found in the lesion surround where reactive astrocytes, activated microglia, and adult precursor cells are abundant (Moon et al., 2002). We previously found enhanced axonal growth in cortical stab wounds in GlcNAc6ST-1−/− mice, but we were not able to investigate the neurological function of these mice at that time (Zhang et al., 2006). In the present study, GlcNAc6ST-1−/− mice exhibited better motor function recovery and enhanced regeneration of the serotonergic descending raphespinal tract axons and CST axons after spinal cord injury, compared with wild-type mice. In support of these data, we also found that the KS-degrading enzyme keratanase reversed the proteoglycan-mediated inhibition of neurite outgrowth *in vitro*. In light of these results, the present study is the first to demonstrate a possible link between KS and neurological function and indicates that GlcNAc6ST-1−/− mice are a good model for investigating the roles of KS in the CNS.

It is of note that neither CS nor KS was sufficient to inhibit neurite outgrowth *in vitro*. However, CS or KS degradation blocked the inhibitory activity of proteoglycans both from chick brains and mouse brains. These results suggest that KS is required for the proteoglycan-mediated inhibition of neurite outgrowth. To our surprise, the effect of KS degradation on this inhibition was comparable to that of CS degradation. Thus, it will be interesting to ask whether KS degradation also promotes functional recovery after neuronal injuries as CS degradation does.

Among the numerous methods available to assess the recovery of locomotor functions, the Basso, Beattie, and Bresnahan (BBB) locomotor scale is a popular choice, because it measures functional changes in voluntary hindlimb movements. In this study, we first used the BBB locomotor scale using five mice in each group, and although we found a slight difference in recovery between the GlcNAc6ST-1−/− mice and controls, the difference did not reach the level of statistical significance ($p = 0.07$; data not

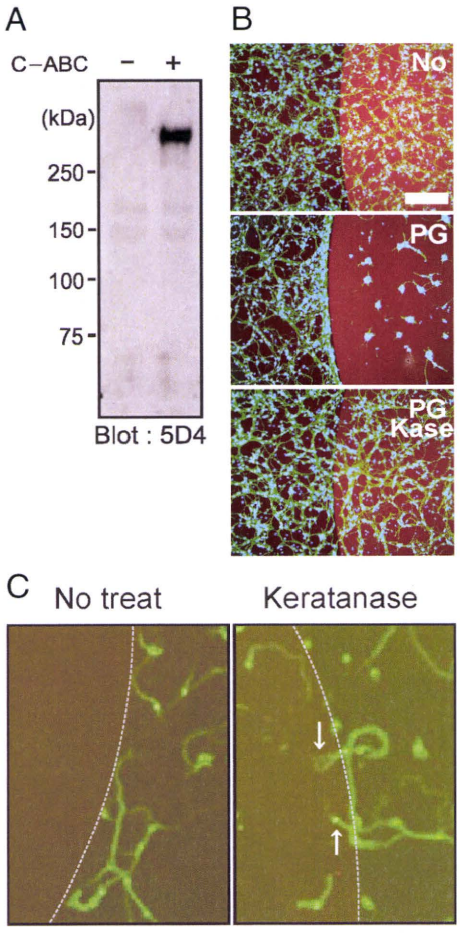

Figure 8. Spot assay. ***A***, Proteoglycans from mouse brain were subjected to Western blot analysis. Note that C-ABC treatment revealed KS epitopes. ***B***, ***C***, Spot assay. Mouse brain proteoglycans at 3 μg/ml were spotted, and primary granular neurons from the rat cerebellum were seeded. Proteoglycans inhibited neurite entry into the spot, whereas keratanase treatment allowed entry. Different cell numbers were used for ***B*** and ***C*** (1.0×10^6 or 1.0×10^5 per well, respectively). Scale bar, 100 μm.

shown). Several locomotor parameters recover differently in mice than in other species (e.g., coordination and paw position recover simultaneously, trunk stability improves earlier, and trunk and hindlimb spasms occur later). These differences limit the sensitivity of the BBB for mice and necessitate a ranking of locomotor attributes unique to mice. To overcome this limitation, a BMS scale was developed for mice (Basso et al., 2006); we applied this locomotor scale using seven mice in each group for 8 weeks and detected a significantly better recovery in the GlcNAc6ST-1−/− mice than in the wild-type controls (Fig. 3*D*). This result was consistent with the footfall, footprint, and motor-evoked potential results. Collectively, the above findings led us to conclude that functional recovery was promoted in GlcNAc6ST-1−/− mice.

The findings of the motor-evoked potential test were consistent with those of the footfall test, footprint test, and BMS scoring. Because the motor-evoked potential test uses only the combination of electric stimulus and response, it can be objectively evaluated. It has recently been shown that motor-evoked potentials have good sensitivity for recording reductions in central conduction latencies (Pluchino et al., 2003; Biffi et al., 2004). In the present study, the responses showed normal configurations, but latency was delayed in the wild-type mice. These electrophysiological data support the idea that the functional recovery of GlcNAc6ST-1−/− mice is remarkably enhanced. However, there may be numerous mechanisms underlying these differences in latency: the conduction differences could be mediated not only by differences in axon regrowth or myelination but also by synaptic reorganization, such as synaptic sprouting, activation of silent synapses, and biochemical synaptic strengthening. Moreover, the type of stimulation used could have activated many descending axon tracts, including not only the CST but also other tracts, such as the rubrospinal, vesitbulospinal, reticulospinal, and propriospinal tracts.

In the present study, we found that most PDGFr-positive cells and a portion of the Iba1-positive cells were KS positive at 7 d after spinal cord injury (Fig. 1). We also found that a portion of the Iba1-positive cells were also KS positive at 3 d, a time point at which most of the Iba1-positive cells were expected to be resident microglia, not macrophages (data not shown). Consistent with this, we have recently reported that primary cultured microglia express KS, and this expression is enhanced by TGF-β, a microglia-activating cytokine usually induced after neuronal injuries (Yin et al., 2009). Considering these results together, it is most likely that, in addition to oligodendrocyte precursor cells (PDGFr positive), activated microglia are a main source of KSPG.

Regarding the reduction of glial scarring in GlcNAc6ST-1−/− mice, whether or not this phenomenon assisted in the functional recovery of these mice is a subject for future debate. Although it is known that glial scars formed in part by reactive astrocytes inhibit axonal sprouting and functional restoration after spinal cord injury (Menet et al., 2003), reactive astrocytes support repair of the blood–brain barrier, prevent inflammatory cell infiltration, and protect neurons and oligodendrocytes (Bush et al., 1999; Faulkner et al., 2004). At least in the subacute phase (within 2 weeks after spinal cord injury), the accumulation of reactive astrocytes helps to repair tissue and restore function (Okada et al., 2006). In this context, our findings are complex. That is, we found that the reactive astrocyte accumulation was significantly lower in GlcNAc6ST-1−/− mice than wild-type mice both at 1 and 4 weeks after injury, whereas the collagen deposition of the GlcNAc6ST-1−/− mice was lower only 4 weeks after injury. It is known that the reactive astrocytes and cells invading into the lesion (i.e., fibroblasts, meningeal cells, and Schwann cells) produce extracellular matrix, including collagen IV (Schwab and Bartholdi, 1996; Fawcett and Asher, 1999; Condic and Lemons, 2002; Buss et al., 2007). However, the influence of collagen IV expression on plasticity and regeneration at the lesion site *in vivo* has been controversial and remains to be elucidated (Shiga and Oppenheim, 1991; Stichel et al., 1999; Weidner et al., 1999; Buss et al., 2007). Thus, our present study has, at least, demonstrated a close association between diminished KS expression and suppressed reactive astrocyte accumulation and collagen IV deposition, although the underlying mechanisms are still elusive.

KS seems to be the most important factor in accounting for the phenotype of GlcNAc6ST-1−/− mice in this study, but we need to exclude the possibility that sulfation modifications on other sugar structures are mediated by GlcNAc6ST-1 and play a role in neuronal function. Other than KS, the only product of GlcNAc6ST-1 thus far identified is sialyl 6-sulfo Le^X, which is a determinant of L-selectin and plays a critical role in lymphocyte recruitment (Uchimura K et al., 2004). GlcNAc sulfation of sialyl 6-sulfo Le^X is mediated either by GlcNAc6ST-1 or -2 (Hemmerich et al., 2001; Uchimura et al., 2004). GlcNAc6ST-1−/− mice show reduced lymphocyte homing to lymph

nodes, and mice doubly deficient in GlcNAc6ST-1 and -2 show significantly greater reduction of lymphocyte homing (Uchimura et al., 2004, 2005; Kawashima et al., 2005). However, we observed a similar degree of CD11b-positive inflammatory cell infiltration in wild-type and GlcNAc6ST-1−/− mice. Therefore, it is not likely that sialyl 6-sulfo Le^X was responsible for the difference in motor function between the wild-type and GlcNAc6ST-1−/− mice in the present study. Furthermore, we obtained evidence that the KS-degrading enzyme keratanase promotes neurite outgrowth, which is inhibited by proteoglycans. Together, our data strongly suggest that the GlcNAc6ST-1 product KS plays a critical role in functional disturbance after spinal cord injury.

References

Akama TO, Nishida K, Nakayama J, Watanabe H, Ozaki K, Nakamura T, Dota A, Kawasaki S, Inoue Y, Maeda N, Yamamoto S, Fujiwara T, Thonar EJ, Shimomura Y, Kinoshita S, Tanigami A, Fukuda MN (2000) Macular corneal dystrophy type I and type II are caused by distinct mutations in a new sulphotransferase gene. Nat Genet 26:237–241.

Basso DM, Fisher LC, Anderson AJ, Jakeman LB, Mctigue DM, Popovich PG (2006) Basso mouse scale for locomotion detects differences in recovery after spinal cord injury in five common mouse strains. J Neurotrauma 23:635–659.

Biffi A, De Palma M, Quattrini A, Del Carro U, Amadio S, Visigalli I, Sessa M, Fasano S, Brambilla R, Marchesini S, Bordignon C, Naldini L (2004) Correction of metachromatic leukodystrophy in the mouse model by transplantation of genetically modified hematopoietic stem cells. J Clin Invest 113:1108–1110.

Borisoff JF, Chan CC, Hiebert GW, Oschipok L, Robertson GS, Zamboni R, Steeves JD, Tetzlaff W (2003) Suppression of Rho-kinase activity promotes axonal growth on inhibitory CNS substrates. Mol Cell Neurosci 2:405–416.

Bradbury EJ, Moon LD, Popat RJ, King VR, Bennett GS, Patel PN, Fawcett JW, McMahon SB (2002) Chondroitinase ABC promotes functional recovery after spinal cord injury. Nature 416:636–640.

Bush TG, Puvanachandra N, Horner CH, Polito A, Ostenfeld T, Svendsen CN, Mucke L, Johnson MH, Sofroniew MV (1999) Leukocyte infiltration, neuronal degeneration, and neurite outgrowth after ablation of scar-forming, reactive astrocytes in adult transgenic mice. Neuron 23:297–308.

Buss A, Pech K, Kakulas BA, Martin D, Schoenen J, Noth J, Brook GA (2007) Growth-modulating molecules are associated with invading Schwann cells and not astrocytes in human traumatic spinal cord injury Brain 130:940–953.

Condic ML, Lemons ML (2002) Extracellular matrix in spinal cord regeneration: getting beyond attraction and inhibition. Neuroreport 13:37–48.

De Winter F, Holtmaat AJ, Verhaagen J (2002) Neuropilin and class 3 semaphorins in nervous system regeneration. Adv Exp Med Biol 515:115–139.

Faulkner RJ, Julia E. Herrmann, Michael J. Woo, Keith E. Tansey, Ngan B. Doan, Michael V. Sofroniew (2004) Reactive Astrocytes Protect Tissue and Preserve Function after Spinal Cord Injury. J Neurosci 24:2143–2155.

Fawcett JW, Asher RA (1999) The glial scar and central nervous system repair. Brain Res Bull 49:377–391.

Filbin MT (2003) Myelin-associated inhibitors of axonal regeneration in the adult mammalian CNS. Nat Rev Neurosci 4:703–713.

Geisert EE Jr, Bidanset DJ (1993) A central nervous system keratan sulfate proteoglycan: localization to boundaries in the neonatal rat brain. Brain Res Dev Brain Res 75:163–173.

Grimpe B, Silver J (2004) Novel DNA enzyme reduces glycosaminoglycan chains in the glial scar and allows microtransplanted dorsal root ganglia axons to regenerate beyond lesions in the spinal cord. J Neurosci 24:1393–1397.

Habuchi H, Habuchi O, Uchimura K, Kimata K, Muramatsu T (2006) Determination of substrate specificity of sulfotransferases and glycosyltransferases (proteoglycans). Methods Enzymol 416:225–243.

Hemmerich S, Bistrup A, Singer MS, van Zante A, Lee JK, Tsay D, Peters M, Carminati JL, Brennan TJ, Carver-Moore K, Leviten M, Fuentes ME, Ruddle NH, Rosen SD (2001) Sulfation of L-selectin ligands by an HEV-restricted sulfotransferase regulates lymphocyte homing to lymph nodes. Immunity 15:237–247.

Jones LL, Tuszynski MH (2002) Spinal cord injury elicits expression of keratan sulfate proteoglycans by macrophages, reactive microglia, and oligodendrocyte progenitors. J Neurosci 22:4611–4624.

Kaneko M, Kubo T, Hata K, Yamaguchi A, Yamashita T (2007) Repulsion of cerebellar granule neurons by chondroitin sulfate proteoglycans is mediated by MAPK pathway. Neurosci Lett 423:62–67.

Kawashima H, Petryniak B, Hiraoka N, Mitoma J, Huckaby V, Nakayama J, Uchimura K, Kadomatsu K, Muramatsu T, Lowe JB, Fukuda M (2005) N-acetylglucosamine-6-O-sulfotransferases 1 and 2 cooperatively control lymphocyte homing through L-selectin ligand biosynthesis in high endothelial venules. Nat Immunol 6:1096–1104.

Kim JE, Liu BP, Park JH, Strittmatter SM (2004) Nogo-66 receptor prevents raphespinal and rubrospinal axon regeneration and limits functional recovery from spinal cord injury. Neuron 44:439–451.

King CE, Canty AJ, Vickers JC (2001) Alterations in neurofilaments associated with reactive brain changes and axonal sprouting following acute physical injury to the rat neocortex. Neuropathol Appl Neurobiol 27: 115–126.

Kitayama K, Hayashida Y, Nishida K, Akama TO (2007) Enzymes responsible for synthesis of corneal keratan sulfate glycosaminoglycans. J Biol Chem 282:30085–30096.

Liesi P, Kauppila T (2002) Induction of type IV collagen and other basement-membrane-associated proteins after spinal cord injury of the adult rat may participate in formation of the glial scar. Exp Neurol 173:31–45.

Massey JM, Hubscher CH, Wagoner MR, Decker JA, Amps J, Silver J, Onifer SM (2006) Chondroitinase ABC digestion of the perineuronal net promotes functional collateral sprouting in the cuneate nucleus after cervical spinal cord injury. J Neurosci 26:4406–4414.

McGee AW, Strittmatter SM (2003) The Nogo-66 receptor: focusing myelin inhibition of axon regeneration. Trends Neurosci 26:193–198.

Menet V, M. Prieto, A. Privat, M. Giménez y Ribotta (2003) Axonal plasticity and functional recovery after spinal cord injury in mice deficient in both glial fibrillary acidic protein and vimentin genes. Proc Natl Acad Sci U S A 100:8999–9004.

Moon LD, Asher RA, Rhodes KE, Fawcett JW (2001) Regeneration of CNS axons back to their target following treatment of adult rat brain with chondroitinase ABC. Nat Neurosci 4:465–466.

Moon LD, Asher RA, Rhodes KE, Fawcett JW (2002) Relationship between sprouting axons, proteoglycans and glial cells following unilateral nigrostriatal axotomy in the adult rat. Neuroscience 109:101–117.

Mueller BK, Mack H, Teusch N (2005) Rho kinase, a promising drug target for neurological disorders. Nat Rev Drug Discov 4:387–398.

Neumann S, Woolf CJ (1999) Regeneration of dorsal column fibers into and beyond the lesion site following adult spinal cord injury. Neuron 23:83–91.

Okada S, Nakamura M, Katoh H, Miyao T, Shimazaki T, Ishii K, Yamane J, Yoshimura A, Iwamoto Y, Toyama Y, Okano H (2006) Conditional ablation of Stat3 or Socs3 discloses a dual role for reactive astrocytes after spinal cord injury. Nat Med 12:829–834.

Pluchino S, Quattrini A, Brambilla E, Gritti A, Salani G, Dina G, Galli R, Del Carro U, Amadio S, Bergami A, Furlan R, Comi G, Vescovi AL, Martino G (2003) Injection of adult neurospheres induces recovery in a chronic model of multiple sclerosis. Nature 422:688–694.

Ruoslahti E (1996) Brain extracellular matrix. Glycobiology 6:489–492.

Schwab ME (2004) Nogo and axon regeneration. Curr Opin Neurobiol 14:118–124.

Schwab ME, Bartholdi D (1996) Degeneration and regeneration of axons in the lesioned spinal cord. Physiol Rev 76:319–370.

Shiga T, Oppenheim RW (1991) Immunolocalization studies of putative guidance molecules used by axons and growth cones of intersegemental interneurons in the chick embryo spinal cord. J Comp Neurol 310:234–252.

Silver J, Miller JH (2004) Regeneration beyond the glial scar. Nat Rev Neurosci 5:146–156.

Stichel CC, Hermanns S, Luhmann HJ, Lausberg F, Niermann H, D'Urso D, Servos G, Hartwig HG, Müller HW (1999) Inhibition of collagen IV deposition promotes regeneration of injured CNS axons. Eur J Neurosci 11:632–646.

Tetzlaff W, Bisby MA (1989) Neurofilament elongation into regenerating facial nerve axons. Neuroscience 29:659–666.

Uchimura K, Kadomatsu K, El-Fasakhany FM, Singer MS, Izawa M, Kannagi R, Takeda N, Rosen SD, Muramatsu T (2004) N-acetylglucosamine 6-O-sulfotransferase-1 regulates expression of L-selectin ligands and lymphocyte homing. J Biol Chem 279:35001–35008.

Uchimura K, Gauguet JM, Singer MS, Tsay D, Kannagi R, Muramatsu T, von Andrian UH, Rosen SD (2005) A major class of L-selectin ligands is eliminated in mice deficient in two sulfotransferases expressed in high endothelial venules. Nat Immunol 6:1105–1113.

Ughrin YM, Chen ZJ, Levine JM (2003) Multiple regions of the NG2 proteoglycan inhibit neurite growth and induce growth cone collapse. J Neurosci 23:175–186.

Weidner N, Grill RJ, Tuszynski MH (1999) Elimination of basal lamina and the collagen "scar" after spinal cord injury fails to augment corticospinal tract regeneration. Exp Neurol 160:40–50.

Widenfalk J, Lundströmer K, Jubran M, Brene S, Olson L (2001) Neurotrophic factors and receptors in the immature and adult spinal cord after mechanical injury or kainic acid. J Neurosci 21:3457–3475.

Yin J, Sakamoto K, Zhang H, Ito Z, Imagama S, Kishida S, Natori T, Sawada M, Matsuyama Y, Kadomatsu K (2009) Transforming growth factor-beta1 upregulates keratan sulfate and chondroitin sulfate biosynthesis in microglia after brain injury. Brain Res 1263:10–22.

Zhang H, Muramatsu T, Murase A, Yuasa S, Uchimura K, Kadomatsu K (2006) N-Acetylglucosamine 6-O-sulfotransferase-1 is required for brain keratan sulfate biosynthesis and glial scar formation after brain injury. Glycobiology 16:702–710.

Uchida et al. BMC Neuroscience 2010, 11:84
http://www.biomedcentral.com/1471-2202/11/84

BMC Neuroscience

RESEARCH ARTICLE Open Access

Microarray analysis of expression of cell death-associated genes in rat spinal cord cells exposed to cyclic tensile stresses in vitro

Kenzo Uchida*[1], Hideaki Nakajima[1], Takayuki Hirai[1], Takafumi Yayama[1], Ke-Bing Chen[1], Shigeru Kobayashi[1], Sally Roberts[2], William E Johnson[2] and Hisatoshi Baba[1]

Abstract

Background: The application of mechanical insults to the spinal cord results in profound cellular and molecular changes, including the induction of neuronal cell death and altered gene expression profiles. Previous studies have described alterations in gene expression following spinal cord injury, but the specificity of this response to mechanical stimuli is difficult to investigate in vivo. Therefore, we have investigated the effect of cyclic tensile stresses on cultured spinal cord cells from E15 Sprague-Dawley rats, using the FX3000® Flexercell Strain Unit. We examined cell morphology and viability over a 72 hour time course. Microarray analysis of gene expression was performed using the Affymetrix GeneChip System®, where categorization of identified genes was performed using the Gene Ontology (GO) and Kyoto Encyclopedia of Genes and Genomes (KEGG) systems. Changes in expression of 12 genes were validated with quantitative real-time reverse transcription polymerase chain reaction (RT-PCR).

Results: The application of cyclic tensile stress reduced the viability of cultured spinal cord cells significantly in a dose- and time-dependent manner. Increasing either the strain or the strain rate independently was associated with significant decreases in spinal cord cell survival. There was no clear evidence of additive effects of strain level with strain rate. GO analysis identified 44 candidate genes which were significantly related to "apoptosis" and 17 genes related to "response to stimulus". KEGG analysis identified changes in the expression levels of 12 genes of the mitogen-activated protein kinase (MAPK) signaling pathway, which were confirmed to be upregulated by RT-PCR analysis.

Conclusions: We have demonstrated that spinal cord cells undergo cell death in response to cyclic tensile stresses, which were dose- and time-dependent. In addition, we have identified the up regulation of various genes, in particular of the MAPK pathway, which may be involved in this cellular response. These data may prove useful, as the accurate knowledge of neuronal gene expression in response to cyclic tensile stress will help in the development of molecular-based therapies for spinal cord injury.

Background

Mechanical stresses applied to the spinal cord can potentially induce profound and irreversible paresis, secondary to induced pathological changes such as dysfunction and loss of neurons, impairment of neuronal cell survival mechanisms and protein synthesis, neuronal cell necrosis and apoptosis [1,2]. Examples of such mechanically induced spinal cord damage include not only spinal cord compression but distraction insult [3,4]; however, it is likely that tensile stresses form an important part of many injuries of the spinal cord. The primary mechanical event, which may occur in less than a second, can initiate a cascade of molecular and cellular events such as changes in gene expression, which may then influence cell function over minutes to hours or a much longer period. For example, transient disruption of Ca^{2+} homeostasis may be an early event in a series of aberrant signaling cascades that ultimately lead to cellular dysfunction or cell death. Extended consequences of this molecular cascade include changes in gene expression levels that are necessary for cell recovery or cell death [5-8].

* Correspondence: kuchida@u-fukui.ac.jp
[1] Department of Orthopaedics and Rehabilitation Medicine, Fukui University Faculty of Medical Sciences, Shimoaizuki 23, Matsuoka, Fukui 910-1193, Japan
Full list of author information is available at the end of the article

Changes in the expression of several immediate early response genes have been documented in various in vivo models of spinal cord injury using microarray analysis [9-11]. These included the up regulation of transcription factors, suggesting that the expression of many other genes is potentially regulated after traumatic insult. Indeed, the differential and post-traumatic expression levels of several genes have been explored in vivo in an attempt to stabilize, both biologically and functionally, the spinal cord once injured [12,13]. However, these in vivo experimental settings for studying the response of neuronal systems to mechanical injury suffer from several disadvantages over in vitro experimentation. For example, mechanical stress can cause additional or unexpected tissue or cell reactions such as activation of resident inflammatory cells or invasion of foreign cells from the periphery [14]. The complexity of the in vivo situation may also result in a limited accessibility to specific areas of tissue or cell type of interest, preventing real-time and spatial measurement of biological or mechanical parameters [15]. Thus, in vitro models of the spinal cord stimuli can be useful to gain a better understanding of the specific neuronal response to mechanical stress.

One approach to determine the pathophysiology of mechanical-stress-related spinal cord damage is to investigate the in vitro response of neuronal cells to loading. The use of neuronal cell culture models allows for better control of the extracellular environment, is relative easy to manipulate, and permits for repeated access to neural cells for specific analysis. The spinal cord and neurons are always subjected to mechanical stress including tensile stresses, during spine movement. Longitudinal vertebral distraction and the physiological tension zone [16] of the spinal cord are closely correlated each other when the spine is subjected to flexural positioning [17,18] and excessive kyphosis in the thoracic vertebrae [19]. The Flexercell Strain Unit (FX3000®, Flexercell International, Hillsborough, NC) is a cell-stretching apparatus that allows application of cyclic tensile force to cultured cells. The system has been used to elucidate the mechanism of mechanical signaling in various types of cells [20-22]. In our previous study using this equipment [23], we investigated the in vitro effects of cyclic tensile stress on cultured spinal cord cells, with a special focus on the expressions of neurotrophins and their receptor genes. The results of that study showed that the application of tensile stress increased the expression levels of nerve growth factor, brain-derived neurotrophic factor, trkB, p75 neurotrophin receptor (p75NTR), glial cell line-derived neurotrophic factor, and caspase-9 mRNAs in the acute phase, followed by increased lactate dehydogenase release and induction of necrotic cell death. These findings led us to investigate further the expression of several genes related to cell death in cultured spinal cord cells under cyclic tensile stress.

The present study was thus designed to examine further the molecular changes and gene expression profiles in cultured spinal cord cells using the above cell-stretching apparatus and DNA microarray technology in order to provide a more complete picture of the changes in the expression of specific genes involved in neuronal response to cyclic tensile stress.

Results

Cyclic tensile stress induced spinal cord cell death

Under the condition of 10% tensile strain (typically found in spinal cord injuries [19]) at a frequency of 0.5 Hz (Figure 1A, B), the proportion of living green-stained spinal cord cells decreased in a time-dependent manner, whereas that of dead red-stained cells increased simultaneously. Transmission Electron Microscopy (TEM) examination showed that all cells at 0 hours appeared viable, with large nuclei, and dotted with chromatin and an abundant rough endoplasmic reticulum. In contrast, in cultures subjected to a tensile stress of 10% strain at 0.5 Hz some cells appeared to show deformity of the nuclei and cytoplasm at 6 hours, and chromatin condensation and fragmentation were observed at 24 hours. These morphological changes were indicative of the start of apoptosis and progressed at 48 hours (Figure 1C).

The cell survival rate of cultures under this cyclic strain as a proportion of that of non strained cultures decreased from 83 ± 24% at 2 hours to 72 ± 19% at 6 hours, 53 ± 15% at 12 hours, 48 ± 14% at 24 hours, 41 ± 9% at 48 hours, and 40 ± 11% at 72 hours (Figure 2A). This decrease in cell survival became significant after 6 hours. Figure 2B shows the cell survival rates as a % of that seen in cultures subjected to a designated standard tensile stress, i.e. 10% strain and 0.5 Hz, after 6 hours at the three different strain levels of 5%, 10%, and 15% and the two different strain rates of 0.5 Hz and 1 Hz. The cell survival rate in cultures subjected to a 10% strain but at a frequency of 1 Hz was significantly lower than that seen at this standard level. Therefore, increasing the strain rate independently of the strain level was associated with increased spinal cord cell death. Conversely, the cell survival rate in cultures subjected to a 15% strain level at a frequency of 0.5 Hz was also significantly lower than that seen at the standard level. Therefore, increasing the strain level independently of the strain rate was also associated with increased spinal cord cell death. There was no clear evidence of additive effects of strain level with strain rate.

Cluster analysis of gene expression profiles

There was altered expression of 3,412 genes after the application of a cyclic tensile stress of 10% at 0.5 Hz. These 3, 412 genes were profiled using hierarchical clus-

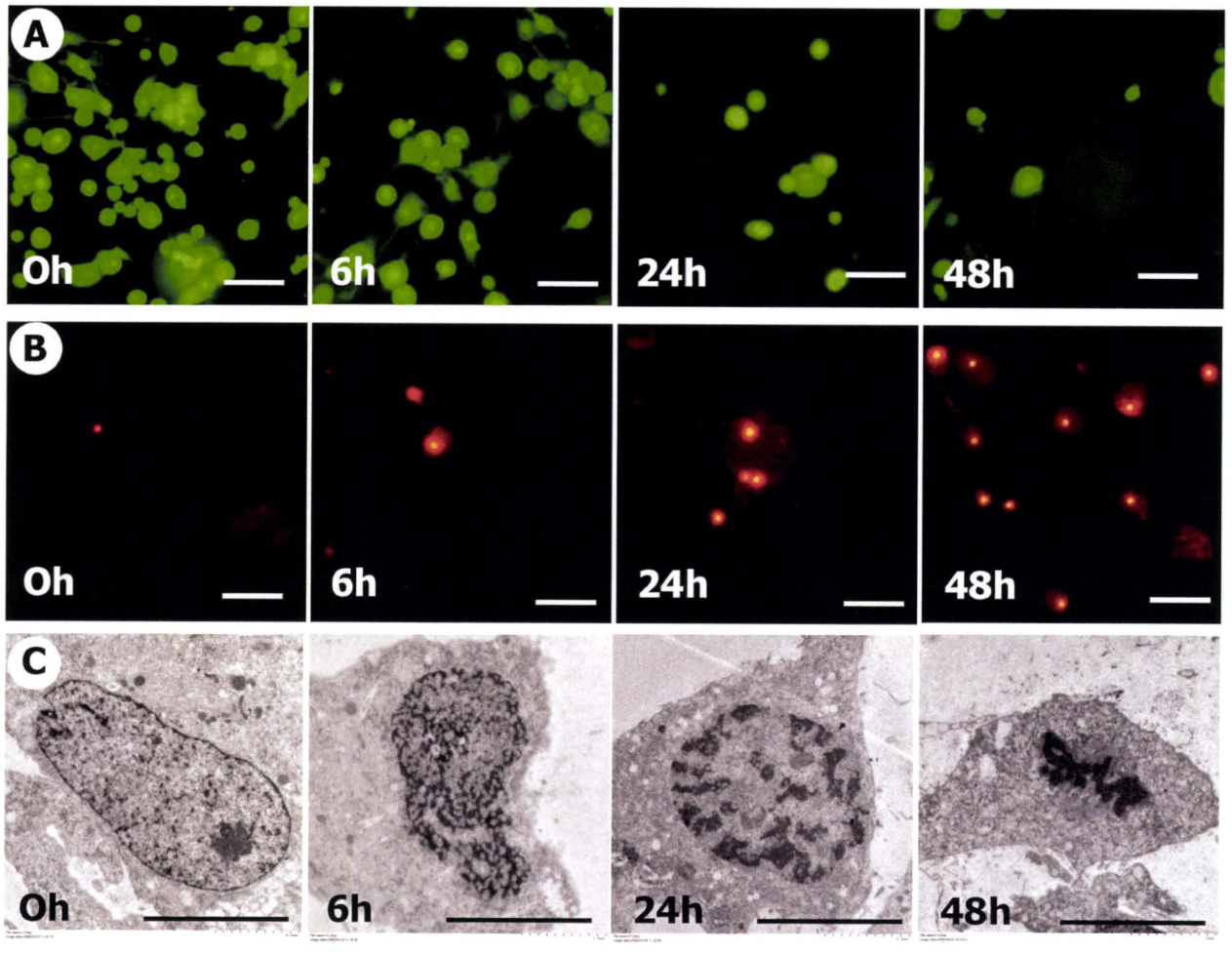

Figure 1 The application of cyclic tensile stress induced apoptotic cell death in spinal cord cells. Representative serial photomicrographs are shown of cells exposed to a tensile stress of 10% strain at 0.5 Hz at 0, 6, 24, and 48 hours (A, B). The number of green-stained living cells decreased (A: top row) while the number of red-strained dead cells increased (B: middle row) in a time-dependent manner during cyclic tensile stress application. Transmission electron microscopy (TEM) examination (C: bottom row) showed that all cells at 0 hour appeared viable, with large nuclei, and dotted with chromatin and abundant rough endoplasmic reticulum, while some cells at 6 hours showed deformity of nuclei and cytoplasm. TEM at 24 hours showed some cells with condensed and fragmented nuclei and condensed chromatin, and the change progressed at 48 hours (C: bottom row). Bar = 100 μm (A, B), 50 μm (C).

ter analysis, based on similarities among their expression patterns in a time course manner. Accordingly, they were divided into 6 clusters (Figure 3). Cluster 1 comprised 67 genes, cluster 2 comprised 102 genes, cluster 3 comprised 1,240 genes, cluster 4 comprised 355 genes, cluster 5 comprised 499 genes, and cluster 6 comprised 1,149 genes. As shown, genes of clusters 1, 2 and 3 were upregulated in a time-dependent manner under cyclic tensile stress, whereas those of cluster 4 were upregulated in a time-independent manner. Genes of clusters 5 and 6 were downregulated in a time-dependent manner under cyclic tensile stress during the 72 hours.

Identification of upregulated genes through Gene Ontology (GO) analysis

Based on the results of clustering analysis, we tested the genes by all GO terms within the biological process in each of the clusters 1-6, and subsequently identified the upregulated genes related to cyclic tensile stress among clusters 1, 2 and 3. The gene related to "apoptosis" belongs to cluster 3 significantly among the cluster 1-3 and the gene related to "response to stimulus" belonged to cluster 1 significantly among the cluster 1-3. Candidate genes related significantly to "apoptosis" among the terms of a biological process were 44 genes in cluster 3, and those significantly related to "response to stimulus" were

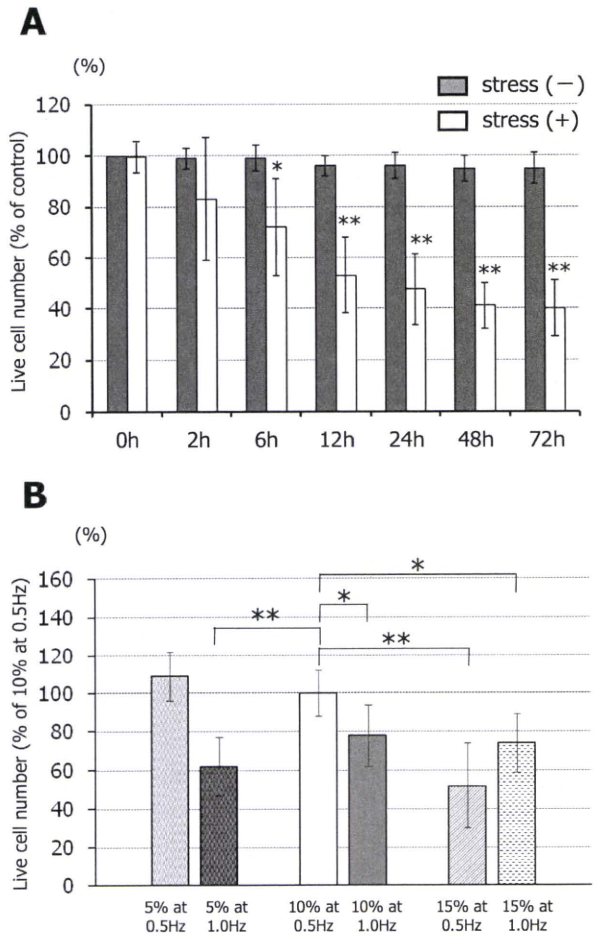

Figure 2 The survival rate of spinal cord cells was dependent on the level, frequency and duration of the applied tensile strain. The survival rate (%) of living cells during the application of a standardized cyclic tensile stress (10%, 0.5 Hz) compared with stress-free baseline (A). Gray bar: stress-free condition; white bar: cyclic tensile stress condition. The survival rate (%) of living cells after 6 hours at three different strain levels of 5%, 10%, and 15% and two different strain frequencies of 0.5 Hz and 1 Hz compared with that at the standardized strain level of 10% at 0.5 Hz frequency (B). Data are expressed as mean ± SEM of 6 experiments. *P < 0.05, **P < 0.01.

17 genes in cluster 1. These genes are listed in Tables 1 and 2, including the relative signal intensity, which was expressed relative to that at 0 hours (boldface show more than 2-fold). Forty-four genes related to "apoptosis" were expressed in the early phase (cluster 3), whereas 17 genes related to "response to stimulus" were expressed in the late phase (cluster 1).

Identification of upregulated genes using Kyoto Encyclopedia of Genes and Genomes (KEGG) analysis

Based on the results of the clustering analysis, we tested the genes by all KEGG terms in clusters 1, 2 and 3 including those genes which were upregulated in a time-dependent manner under cyclic tensile stress. These pathways with p values < 0.05 are listed in Table 3. Four pathways were significantly included in cluster 1, 3 pathways in cluster 2, and 24 pathways in cluster 3.

Gene-specific real-time reverse transcription polymerase chain reaction (RT-PCR) in MAPK signaling pathway

In further examination of KEGG analysis of cluster 3, which included many of the upregulated genes, we found that the MAPK signaling pathway contained 12 candidate genes among the 15 genes that were significantly upregulated. These genes were calcium channel voltage-dependent L type alpha 1F subunit (Cacnalf or CACN), neurotrophic tyrosine kinase receptor type 2 (Ntrk2 or trkA/B), fibroblast growth factor receptor 2 (Fgfr2 or FGFR), platelet-derived growth factor receptor, beta polypeptide (Pdgfrb or PDGFR), v-raf-leukemia viral oncogene 1 (Raf1 or Raf), guanine nucleotide binding protein (G protein) gamma 12 (Gng12 or G12), dual specificity phosphatase 1 (Dusp1 or MKP), mitogen-activated protein kinase kinase kinase kinase 4 (Map4k4 or HGK), mitogen-activated protein kinase 8 interacting protein 3 (Mapk8ip3 or JIP3), heat shock protein 72 (Hspa 72 or HSP72), growth arrest and DNA-damage-inducible alpha (Gadd45a or GAD D45), and DNA-damage inducible transcript 3 (Ddit3 or GAD D153). To confirm the expression of genes identified using the microarrays, these 12 genes were identified to test differential expression using real time RT-PCR analysis. The mRNA expression levels of PDGFR, G12 was significantly increased from the mid period of application of cyclic tensile stress (12-hour stress duration), while CACN, trkA/B, FGFR, Raf1, MKP, HGK, JIP3, HSP72, GAD D45, and GAD D153 mRNA expression levels increased during the late phase of cyclic tensile stress (24-72 hours duration). In each case these significant upregulations in mRNA expression levels was by at least 2-fold in comparison with the control levels at time 0 (Figure 4).

Discussion

In vitro systems offer several advantages over in vivo systems in the analysis of cellular responses to their mechanical environment, including the precise specification of loading parameters (strain levels and strain rate), control of the extracellular environment (temperature, ion concentration, partial pressure of gases), the relative ease and repeated access of the cells, and simplified administration of pharmacological compounds. By precisely controlling the loading conditions, the quantitative relationship between the severity of mechanical injury and response to the injury can be evaluated [24]. Previous mechanical stimulation studies of neuronal cells using immortalized cell lines reported that the physiological strain conditions of neuronal cells are not as high as osteoblasts or skeletal muscle cells [25]. Rat motoneurons stretched at 11%

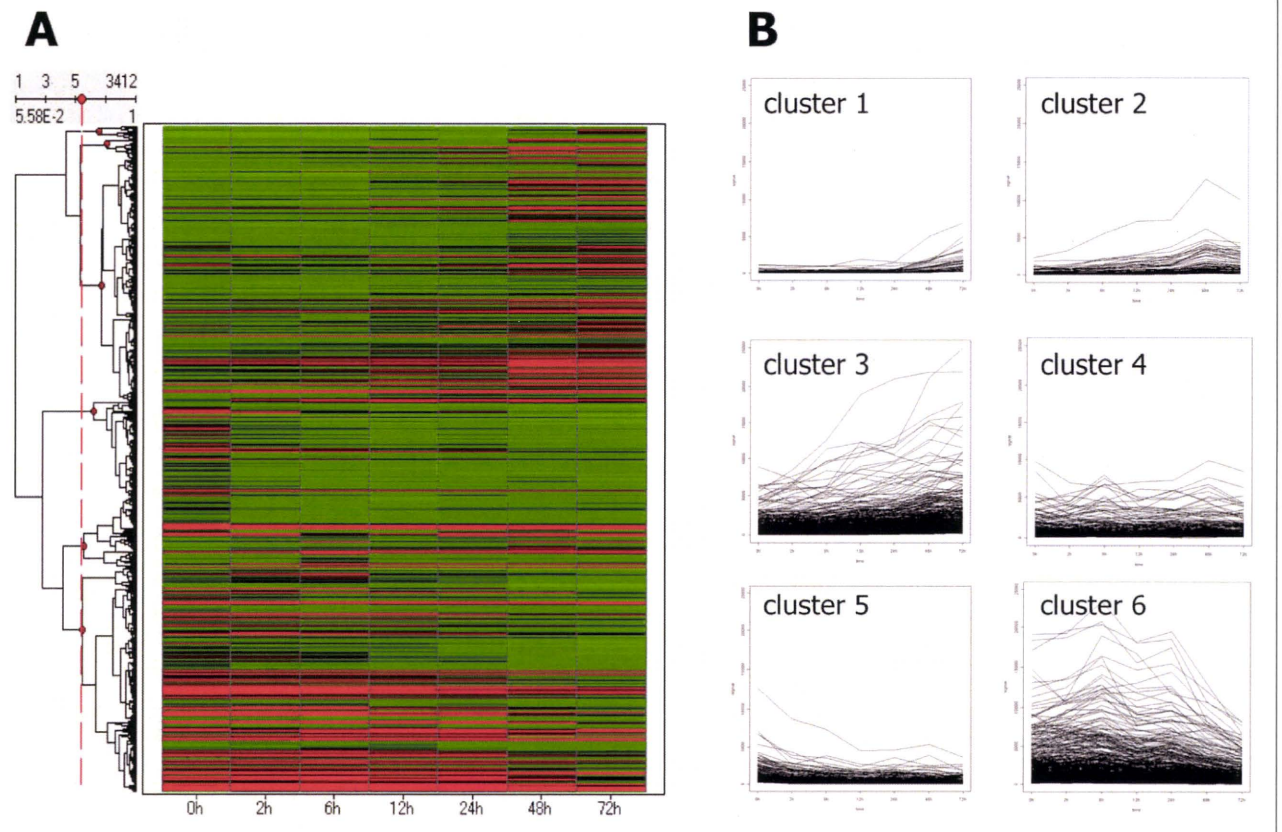

Figure 3 Gene expression profiles in spinal cord cells after the application of cyclic tensile stress. The hierarchial clustering data are presented graphically as a heatmap (A). These genes were subsequently grouped into six subclusters (cluster 1-6) according to the time course of gene expression pattern (B).

strain showed ischemic changes but no mechanical damage [26], whereas at a 6% strain level there were no ischemic changes or mechanical damage [27]. PC12 cells were subjected to cyclic tensile strain levels ranging from 4 to 16% at strain frequencies of 1-2 Hz as physiological mechanical conditions [25]. Based on these reports and considering primary cultured spinal cord cells [23], we selected the range of cyclic tensile stresses most appropriate to our culture system in the present study, and the cells were observed morphologically following application of various tensile strains levels (5%, 10%, and 15%) and strain frequencies (0.5 Hz and 1 Hz) using the Flexercell system. Interestingly, we found a significant decrease in the cell survival rate (%) when cultures were subjected to either a cyclic tensile stress of 5% at 1 Hz or 15% at 0.5 Hz, compared with a cyclic tensile stress at 10% at 0.5 Hz, which was taken as a control level. Our results suggest that both the level of strain applied and frequency of its application influence cell viability. Furthermore the results demonstrate that a higher strain level at a lower strain rate can have a similar effect as a lower strain level at a higher strain rate in neuron-rich spinal cord cells.

To understand the molecular mechanism of neuronal responses to cyclic tensile stress, DNA microarray was employed to identify the specific gene expression patterns in cultured spinal cord cells, and the hierachical clustering algorithm was used in the analysis. Consequently, we found that 44 genes related to "apoptosis" among cluster 3 included the majority of progressively upregulated genes by enrichment analysis using biological process in the GO system. Furthermore, 17 genes related to "response to stimulus" were also identified among those of cluster 1, including most upregulated genes in the late phase after application of cyclic tensile stress. On the other hand, the KEGG/pathway analysis identified different pathways in the upregulated genes in a time-dependent manner in the clusters 1, 2, and 3 which had been identified via the GO system.

A number of investigators have attempted to characterize or determine changes in specific genes and signaling pathways of direct mechanical stress or load using cells from diverse tissues and in vitro models of mechanical trauma. These systems are multifold and can be separated into detection, response, and modulation pathways